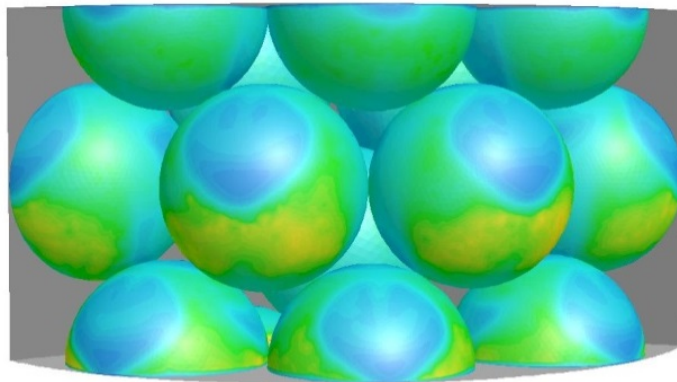


Transient Simulation of Chemical Looping Combustion using Computational Fluid Dynamics

A Major Qualifying Project Report



Zephyr Dana Cady
Andrew Thomas Moscariello
Angela Dawn Simpson



WPI

Transient Simulation of Chemical Looping Combustion using Computational Fluid Dynamics

A Major Qualifying Project Report
Submitted to the Faculty of
WORCESTER POLYTECHNIC INSTITUTE

in partial fulfillment of the requirements for the
degree of Bachelor of Science
in Chemical Engineering

by
Zephyr Dana Cady
Andrew Thomas Moscariello
Angela Dawn Simpson

Date:
April 23, 2013

Submitted to:
Professor Anthony G. Dixon
Worcester Polytechnic Institute

Abstract

Packed bed chemical looping combustion (CLC) reactors are a safer and more sustainable method for creating energy from the combustion of hydrocarbons. This project presents a transient simulation of a CLC reactor using the computational fluid dynamics (CFD) software package Fluent 6.3. Results were obtained for the reduction and oxidation phases of the process, illustrating the expected qualitative trends. This project concludes that CFD software can be effectively used to simulate transient chemical reactions.

Executive Summary

Global warming is an issue that has gained attention in the past decade. A principle contributor to global warming is the release of greenhouse gasses, including carbon dioxide (CO₂). Thus, there has been an increasing focus on reducing carbon emissions. The largest source of carbon emissions is energy production.¹ A majority of energy in the United States is produced through the combustion of fossil fuels such as coal and natural gas.² One alternative to a traditional combustion reactor setup is a chemical looping combustion (CLC) reactor.

A CLC reactor contains catalyst particles which are alternately oxidized then reduced. Typically either packed bed or fluidized bed reactors are used for CLC. In a packed bed reactor, an oxygen source, such as air, is fed. Then a fuel source, such as natural gas or methane, is fed. This type of reactor can produce an easily-captured CO₂ stream and is safer for operation.

Simulations of chemical processes are a valuable tool. They are often the first efforts made while investigating new technologies. Although bench- and pilot-scale experiments provide valuable data, they can be costly and time-consuming. Simulations, however, are a cheaper alternative that still allowed detailed data collection. One common method for simulating detailed transport phenomena and reaction is computational fluid dynamics (CFD) software.

This project used CFD to simulate a packed bed CLC reactor. The goal of the project was to demonstrate transient reaction modeling using the CFD software Fluent[®] 6.3. The model utilized a 120° wall segment model of reactor with 2 mm diameter spherical catalyst particles. The model used a 1.5 million cell mesh. The model was desired to be representative of the

¹ Lawrence Livermore National Laboratory. Estimated US Energy Use in 2011: ~97.3 Quads, 2012. Energy Flow. https://flowcharts.llnl.gov/content/energy/energy_archive/energy_flow_2011/LLNLUSEnergy2011.png (accessed Oct 25, 2012).

² Ibid.

interior of a long reactor that had been undergoing reaction for some time, and was set up accordingly.

User-defined code was written to define reaction kinetics and species transport within the solid catalyst particles. A periodic flow model was solved to obtain a fully-developed turbulent flow profile. Individual non-periodic reaction models were then run on a time-dependent basis for the reduction and oxidation phases of CLC reactions.

Simulation of the reduction reaction phase was successful isothermally over a time span of 0.8 ms with reaction rates lowered to 1% of the original values. An increase in the concentration of combustion products CO_2 and water (H_2O), along with a decrease in the concentration of reactant methane (CH_4) were observed. As expected, an increase in the concentration of reduced catalyst, nickel (Ni), was also observed.

Simulation of the oxidation phase was successful over a time span of 8 ms with reaction rates lowered to 1% of the original values. An increase in the amount of oxidized catalyst, nickel oxide (NiO) was observed along with a decrease in the amount of reduced catalyst, Ni. Both of these results were as expected.

In conclusion, reduction and oxidation phases of looping demonstrated the expected qualitative results. Accurate quantitative results were not obtained, as expected. Computational fluid dynamics software can be used to simulate transient chemical reactions, as illustrated with this example of chemical looping combustion. However, a full, realistically accurate simulation is not easily possible although results display expected qualitative trends.

Table of Contents

Abstract	ii
Executive Summary	iii
Table of Contents	v
Table of Figures	vii
Table of Tables	viii
1. Introduction	1
2. Background	5
2.1 Computational Fluid Dynamics	5
2.2 Chemical Looping	8
2.2.1 Kinetics for Chemical Looping Combustion	8
3. Methodology	10
3.1 Reaction Fundamentals	11
3.1.1 Kinetics and Rate Laws	11
3.1.2 Catalysts	13
3.1.3 Diffusivity	13
3.2 Simulation Model Preliminary Steps	13
3.2.1 Model and Geometry Scaling	14
3.2.2 Periodic Model	16
3.2.3 Reaction Model Set Up	18
3.2.4 Additional Model Parameters	18
3.3 User Defined Scalars and Functions	19
3.4 Transient Modeling	21
3.5 Reduction Phase Reaction Model	22
3.5.1 Bootstrapping	22
3.6 Oxidation Phase Reaction Model	23
3.6.1 Bootstrapping	23
4. Results and Discussion	24
4.1 Periodic Flow	24
4.2 Reduction Phase	27
4.3 Oxidation Phase	33
5. Conclusions and Recommendations	39
5.1 Feasibility of CFD simulation of transient reactions.	39
5.2 Future Research	39
6. Nomenclature	41
Greek Letters	41
Subscript	41
Abbreviations	41
Chemical Formulas	42
7. References	43

Appendix A: Methane Reforming as a Novel Application of Chemical Looping	45
References	47
Appendix B: Heats of Reactions	48
References	53

Table of Figures

Figure 1: Schematic of chemical looping process, using chemical looping combustion as an example.....	2
Figure 2: Schematic of an example chemical looping combustion system (Fan & Li, 2010)	3
Figure 3: Three-dimensional CFD wall-segment model geometry (Boudreau & Rocheleau, 2010).....	6
Figure 4: Particle Mesh in Reaction Model.....	14
Figure 5: Single Center Particle Mesh	15
Figure 6: Location of Central Particles	24
Figure 7: Periodic Flow Model Solution Residuals	25
Figure 8: Convergence History of Static Pressure on top	26
Figure 9: Convergence History of Z Velocity on top.....	26
Figure 10: Contour of Mass Fraction of CH ₄ on Central Particles (Time = 1.48E-3)	28
Figure 11: Contours of Mass Fractions of CH ₄ on Central Particles (Time = 2.28E-3)	28
Figure 12: Contours of Mass Fractions of CO ₂ on Central Particles (Time = 1.48E-3)	29
Figure 13: Contours of Mass Fractions of CO ₂ on Central Particles (Time = 2.28E-3)	29
Figure 14: Contours of Scalar-1: Mass Fractions of H ₂ O on Central Particles (Time = 1.48E-3)	30
Figure 15: Contours of Scalar-1: Mass Fractions of H ₂ O on Central Particles (Time = 2.28E-3)	30
Figure 16: Contours of Scalar-5: Concentrations of Ni on Central Particles (Time = 1.48E-3). 31	
Figure 17: Contours of Static Temperature [K] on Central Particles (Time = 1.88E-3).....	32
Figure 18: Contours of Scalar-5: Non-isothermal Concentrations of Ni on Central Particles (Time = 2.28E-3)	33
Figure 19: Contours of Scalar-5: Concentrations of Ni on Central Particles(Time = 9.23E-3)..	34
Figure 20: Contours of Scalar-5: Concentrations of Ni on Central Particles (Time = 1.723E-2)35	
Figure 21: Contours of Scalar-6: Concentrations of NiO on Central Particles (Time = 9.23E-3)	35
Figure 22: Contours of Scalar-6: Concentrations of NiO on Central Particles (Time = 1.723E-2)	36
Figure 23: Contours of Static Temperature [K] on Central Particles (Time = 9.23E-3).....	37
Figure 24: Contours of Static Temperature [K] on Central Particles (Time = 1.723E-2).....	37
Figure A.1: SMR Process Block Diagram (Molburg & Doctor, 2003)	46

Table of Tables

Table 1: Individual reduction reactions for chemical looping combustion over a nickel catalyst .	9
Table 2: Mass Fractions for Inlet Conditions	17
Table B.1: Reaction Names (Iliuta et al., 2010; Dueso et al., 2012).....	48
Table B.2: Reaction Stoichiometric Coefficients.....	48
Table B.3: Heat Capacity Constants (Perry & Green, 2008; Smith et al., 2005).	49
Table B.4: Heat Capacities of Reaction Species at Various Temperatures.	49
Table B.5: Enthalpies of Reaction Species at Various Temperatures.	50
Table B.6: Standard Enthalpies of Formation of Reaction Species (Perry & Green, 2008; Smith et al., 2005).	50
Table B.7: Enthalpy of Formations of Reaction Species at Various Temperatures.	51
Table B.8: Enthalpies of Reactions for Various Temperatures	52

1. Introduction

As individuals become more conscious of the environment and the finite amount of fossil fuels available, they look towards alternative sources of energy that would still allow them the same comforts and standards of living they currently enjoy. The most energy intensive of these comforts are electricity and transportation. In 2011, 39% of all energy resources used by the United States went into electricity production (Lawrence Livermore National Laboratory, 2012). Electricity is typically generated by producing high pressure steam that is then sent through turbines. The most common method for producing this steam is by combusting hydrocarbons to provide the needed heat. In 2011, 46% of the energy for producing steam in the United States came from coal and 20% came from natural gas (Lawrence Livermore National Laboratory, 2012). Any combustion reaction can produce pollutants and greenhouse gases. A greater emphasis on pollution reduction signals a desire to move towards cleaner ways of producing electricity.

Combustion is the oxidation of a hydrocarbon to produce water (H_2O), carbon dioxide (CO_2), and heat. As with any reaction, there are also unwanted side reactions that produce species like carbon monoxide (CO) and nitrogen oxides (NO_x) if air is used as the oxygen source. NO_x production can be controlled by using an oxygen-rich feed instead of air, and CO production can be reduced by combusting at a higher temperature. However, CO_2 will always be present in product streams. The current challenge, in regards to the environment, is the safe capture and sequestration of CO_2 from combustion. Carbon emissions, specifically carbon dioxide emissions, are the leading contributor to global warming and climate change and, as such, large reductions in the emissions of greenhouse gases, primarily carbon dioxide, are needed to slow the increase of atmospheric concentrations (G8+5 Academies' joint statement, 2009).

One method for controlling CO₂ emissions is to directly capture it from combustion. This task is simplified when a mostly pure CO₂ stream can be produced. Traditional combustion technology is unable to do this. One example of an alternative technology that could be used to produce a pure CO₂ stream from combustion is a chemical looping reactor.

Chemical looping consists of alternately oxidizing and reducing a catalyst particle. The catalyst is often a metal or metal oxide on a support. Common metals include nickel (Ni), copper (Cu), iron (Fe), iron (II, III) oxide (Fe₃O₄) and manganese (II) oxide (MnO) supported by alumina (Al₂O₃), titanium dioxide (TiO₂), bentonite, or zirconium dioxide (ZrO₂) (Fan & Li, 2010). The chosen catalyst particle is alternately exposed to oxidizing and reducing environments where the particle changes between reduced and oxidized states, as shown in Figure 1.

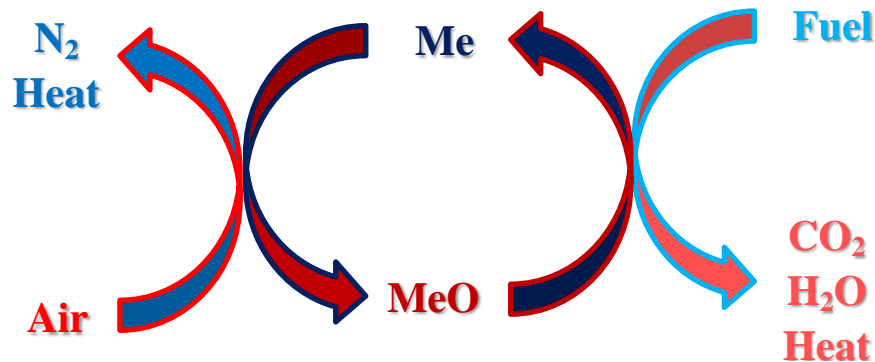


Figure 1: Schematic of chemical looping process, using chemical looping combustion as an example

While Figure 1 illustrates chemical looping combustion there are several applications of interest that can occur in a chemical looping reactor.

Traditionally chemical looping reactors are made up of a circuit of fluidized bed reactors. One reactor acts as the oxidizer and the other as the reducer. Air enters into the oxidizer where the catalyst bonds with oxygen. The catalyst particles are then fed to a second bed that acts as the

reducer where they are reacted with fuel. The reduced particles are then sent back to the first bed where the process is repeated. A schematic of this system is shown in Figure 2.

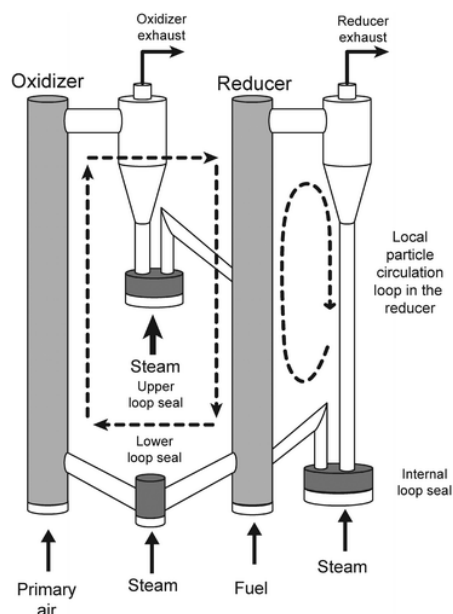


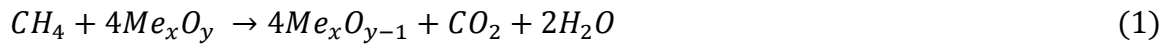
Figure 2: Schematic of an example chemical looping combustion system (Fan & Li, 2010)

Fluidized bed reactors present several areas of concern for chemical looping. The main difficulty faced is catalyst particle degradation. As the particles move through the beds they collide with other particles and the equipment, resulting in loss of particle strength. Eventually pieces of the particles will break off. The fines that can be created in a chemical looping system are difficult to remove from the process stream and pose problems for any downstream equipment as they can damage moving parts. Additionally, particulate handling operations require additional plant employees, raising the operating costs through cost of labor. Alternative reactor designs for performing chemical looping reactions have thus been explored.

Packed bed reactors have been investigated as an alternative means for conducting chemical looping reactions (Noorman et al., 2007). To perform a chemical looping reaction the reactor, packed with catalyst, would be alternately fed an air stream and a fuel stream. This alternating feed would produce oxidizing and reducing environments in the reactor for the

catalyst particle. A packed bed reactor offers benefits over a fluidized bed reactor. Since the catalyst particles are not moved there is little to no particle attrition. The effluent stream can therefore be safely sent to mechanical devices, such as turbines, and avoid a filtration step. For this reason, one application of chemical looping that could utilize packed beds, is chemical looping combustion.

Chemical looping combustion (CLC) indirectly combusts fuel to generate heat (Fan & Li, 2010). CLC reactions are highly exothermic, producing enough heat to be self-sustaining. CLC reactions are of the form (Dueso et al., 2012):



CLC produces a pure CO₂ stream that can be captured and sequestered by condensing the water out of the reactor effluent. It has also been shown that in a packed bed reactor, a high temperature air stream can be produced that can be used to operate a turbine to produce electricity (Noorman et al., 2007). If two reactors are set up in parallel a constant air stream can be obtained (Noorman et al., 2007). Use of chemical looping offers a safer method of combustion, compared to traditional combustion reactors, as the fuel is never in direct contact with the air. Thus, CLC in packed bed reactors offers a suitable alternative method for electricity production.

2. Background

Computer simulations of chemical processes are often the first efforts made towards investigating new technologies. While lab and pilot scale experiments can provide insight into the specifics of a process on the small scale, simulation can provide much more information about the process as a whole. By coupling simulations with small-scale experiments, a significant amount of information can be obtained about a new process to show if the process would be economical, or even feasible at full-scale before any capital is spent on actually building it. This section presents a brief overview of computational fluid dynamics with an explanation of unsteady state simulation. Then a practical application of unsteady state simulation in chemical looping is discussed. The specific kind of chemical looping, combustion, used in the simulations is introduced along with an explanation of the kinetics involved in its reactions.

2.1 Computational Fluid Dynamics

Computational fluid dynamics (CFD) is a set of numerical methods applied to obtain approximate solutions of problems of fluid dynamics and heat transfer (Zikanov, 2010). The growth of computers and processing powers has allowed a related growth in CFD ability (Wendt, 2009). From this growth, CFD has been increasingly used to model processes of fluid flow, heat and mass transfer, and chemical reactions. One CFD software package that can be used to simulate CLC in a fixed bed reactor is Fluent[®]. With chemical looping reactors being unsteady by definition, CLC necessitates an unsteady, and therefore more complex, model. In addition to requiring the simulation to iterate and numerically solve the equations for heat transfer, reaction rates, and mass transfer, along with fluid flow, the simulation will need to obtain a solution that changes with each step forward in time. Stepping the simulation forward in time adds a layer of

complexity to the model, and subsequently requires more time to solve. Due to this complexity, simulations can be performed in a limited fashion, with reactions being added to the simulation slowly, making sure it is still capable of converging before moving further each time.

In a previously studied analysis of steam methane reforming using CFD, a full randomly packed bed was not modeled due to the difficulty of modeling the tubes. This was because of the level of intricacy of their geometry and the computing power needed (Boudreau & Rocheleau, 2010). Shorter pieces of tubing are thus more suitable to model. A 120° wall segment model shown in Figure 3 with symmetry on the sides could be considered only an approximate representation of central catalyst particles and not the entire reactor. For this model a tube-to-particle diameter ratio of four was used.

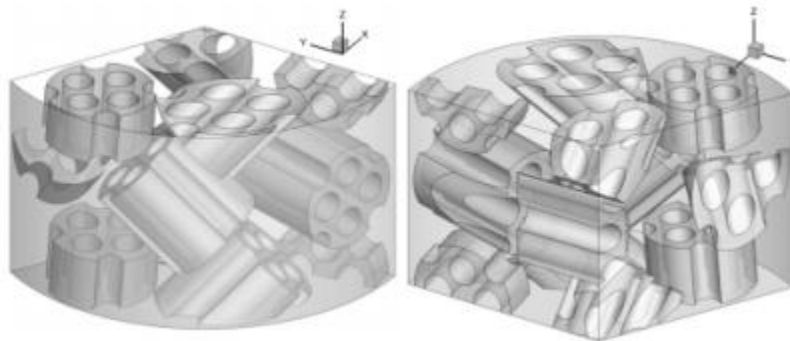


Figure 3: Three-dimensional CFD wall-segment model geometry (Boudreau & Rocheleau, 2010)

Even with advancements in CFD, there are still limitations of processing power and software. Fluent[®] cannot account for diffusion into the catalyst when modeling it as a solid. To allow diffusion, the catalyst particle can be defined as a porous region by modeling the particle as a modified fluid region with additional resistance to flow, achieved by adding extra terms in the momentum balance (Dixon et al., 2010). Adding source terms accounts for reactions that take place in the catalyst particle, with the velocity in the particle fixed to be zero (Dixon et al., 2010). With these specifications, diffusion was allowed; however, there were still limitations that gave incorrect results (Dixon et al., 2010). One deficiency of Fluent[®] was in the convective flux

across the particle-fluid interface that led to inaccurate temperature and species profiles as well as incorrect particle-to-fluid heat transfer coefficients (Dixon et al., 2010). Making use of User Defined Scalars (UDS) can improve these limitations.

Fluent[®] is a program originally developed mainly for mechanical engineering applications. Fluent[®] has been expanding in its ability to model reactions effectively; however, there remain a few limitations. Fluent[®] cannot recognize reactions or mixtures in a solid phase, specifically reactions on the interior surface of a porous catalyst particle. This program design presents a large problem when attempting to model surface-catalyzed reactions. The method used by Boudreau & Rocheleau to work around this issue was to make use of Fluent's[®] capability to read in User Defined Functions and scalars coded in C.

User Defined Scalars (UDS) in Fluent[®] are simple numbers such as temperature, pressure, mass fraction, or concentration. These scalars can be grouped into functions and equations, and implemented in Fluent[®]. Fluent[®] allows the creation of equations known as User Defined Functions (UDF), which can make use of both variables inside Fluent[®] as well as UDSs, and can be used to model any property that is desired, so long as all mathematical relationships and parameters are supplied to Fluent[®]. Fluent[®] has a general built-in system for keeping track of UDF and UDS. Defining UDS and UDF necessitate a thorough mathematical description of all relationships in the created file to assist Fluent[®] in interpreting the code.

The first step in getting around the barrier presented of needing to model reactions and multiple species in the solid phase is to define scalars for mass fractions. Once a method to tell Fluent[®] what is present inside the catalyst particle or on the surface is set, concentrations and subsequently reaction rate equations can then be described. In order to tell Fluent[®] how these reactions vary within the model it is necessary to supply derivatives of each reaction rate with

respect to both temperature and species concentration. Once all of this information is determined, it can be compiled into a file with all the code for how sources of each species are present, and how species are consumed.

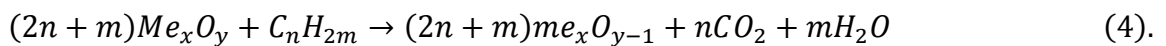
After species are defined through UDS, a problem arises regarding continuity of concentration between the surface or solid and the fluid just outside the solid. Fluent[®] is capable of performing continuity balances but not between UDS and Fluent's[®] built in mass fraction parameters. It therefore becomes necessary to make use of UDF code which checks for where the fluid boundary starts. Fluent[®] can then be told explicitly that the mass fraction on the fluid side is equal to the UDS used to define mass fraction on the solid side.

2.2 Chemical Looping

The main concern when attempting to model chemical looping of any kind is to obtain experimentally determined reaction kinetics, including rate expressions. Heats of reaction, densities, and other species and fluid properties can be estimated with at least some degree of accuracy. In contrast, reaction kinetics cannot, and must be found experimentally.

2.2.1 Kinetics for Chemical Looping Combustion

To provide a mathematical model for the reactions, it is necessary to make use of experimentally determined reaction kinetics found in literature. Kinetics for CLC have been developed by Iliuta et al. for reduction of nickel based oxygen carriers prepared on Al_2O_3 (2010). Multiple side reactions, including those present in reforming, were considered to be significant contributors to the overall combustion reaction, of the form



Oxidation of the metal oxygen carrier is considered to proceed through



Complete combustion occurs through typical combustion reactions in addition to several reactions catalyzed by the nickel. Reduction reactions and side reactions for CLC are shown in Table 1 (Iliuta et al., 2010). Reaction rate examples with derivations are shown in Section 3.1.1.

Table 1: Individual reduction reactions for chemical looping combustion over a nickel catalyst

Reaction	Name and abbreviation
$CH_4 + 2NiO \leftrightarrow 2Ni + 2H_2 + CO_2$	1
$H_2 + NiO \leftrightarrow Ni + H_2O$	2
$CO + NiO \leftrightarrow Ni + CO_2$	3
$CH_4 + NiO \leftrightarrow Ni + 2H_2 + CO$	4
$CH_4 + H_2O \xrightleftharpoons{Ni} CO + 3H_2$	Methane reforming (rf, H ₂ O)
$CH_4 + CO_2 \xrightleftharpoons{Ni} 2CO + 2H_2$	Methane reforming (rf, CO ₂)
$CH_4 + Ni \leftrightarrow Ni \cdot C + 2H_2$	Methane decomposition/deposition (cd)
$CO + 3H_2 \xrightleftharpoons{Ni} CH_4 + H_2O$	Methanation (CH ₄ , m)
$CO + H_2O \xrightleftharpoons{Ni} CO_2 + H_2$	Water Gas Shift (WGS)
$C + CO_2 \xrightleftharpoons{Ni} 2CO$	Gasification (g, CO ₂)
$C + H_2O \xrightleftharpoons{Ni} CO + H_2$	Gasification (g, H ₂ O)

3. Methodology

In order to complete a simulation of transient chemical looping combustion (CLC), many tasks relating to different aspects of the simulation had to be accomplished. Fluent[®] 6.3.26 was used for all simulations in this project. Fluent 6.3.26 was chosen because it models fluid dynamics using the finite volume method, and it allows user defined code. First and foremost, experimentally determined kinetics were obtained and rate laws for the CLC reactions were studied. Once these kinetic parameters were obtained, User Defined Scalars (UDS) were created in order to effectively tell Fluent[®] how the concentrations of the species present in the reactor varied with time. Species source terms for all UDS were written to satisfy mass conservation laws, and were of the form

$$\frac{\partial}{\partial t}(\rho Y_i) + \nabla \cdot (\rho \vec{u} Y_i) = -\nabla \cdot \vec{J}_i + R_i + S_i \quad (6)$$

where ρ is density, Y_i is species mass fraction, \vec{u} is the velocity of the bulk phase, R_i is the net rate of production of species i , S_i is the source term of species i , and J is the diffusive flux determined by the equation

$$\vec{J}_i = -\left(\rho D_{i,m} + \frac{\mu_t}{Sc_t}\right) \nabla Y_i \quad (7)$$

where $D_{i,m}$ is the turbulent diffusivity of species i into the mixture m , μ_t is the turbulent viscosity, and Sc_t is the turbulent Schmidt number (UDS Theory, 2006).

Once all UDFs were coded, simulation work began with obtaining a periodic flow profile from a standalone periodic simulation in order to obtain a reasonable inlet flow profile for the reactor model. A non-periodic reactor simulation was then run to model the reduction phase of looping. Finally, the oxidation phase of looping in a non-periodic reactor model was simulated.

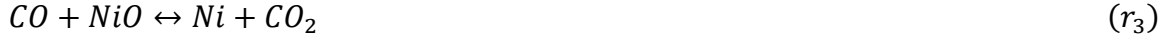
3.1 Reaction Fundamentals

Since CLC was chosen to be the example for demonstrating transient reaction modeling using CFD, reactions occurring under combustion conditions were researched. After some consideration, rates and kinetic parameters for four main reactions were obtained and used for the reduction phase of looping, along with an additional oxidation reaction considered to take place in the oxidation phase of looping. These reactions all were dependent on the concentrations of catalyst surface reaction sites, and were all considered to occur only on the surface of the catalyst particles present in the model, as is shown by the kinetics.

3.1.1 Kinetics and Rate Laws

Rate laws and experimentally determined kinetic parameters were obtained from Iliuta et al. and Dueso et al. for both reduction and oxidation phases of looping (2010; 2012). These kinetics were chosen for their simplicity because they exhibited elementary kinetic rate law behavior. More complicated experimental kinetics, while possibly displaying higher accuracy, would have unnecessarily complicated the process, and were avoided. Although there were several reaction rates presented that corresponded to side reactions thought to be occurring, as shown in Table 1, these reactions were not considered in the model (Iliuta et al., 2010). It was desirable for this project to focus only on solid-phase reactions, taking place on the catalyst surface, and catalyzed reactions taking place in the gas-phase were not considered. Ignoring these gas-phase side reactions was an approximation made in order to simplify the model. In order to ensure better model convergence, only the four main combustion reactions for the reduction phase were used. The net reaction obtained from these four reactions is general combustion, making it appropriate to use only these four for the simulation. For the oxidation phase of looping, only a single oxidation reaction was considered to take place.

The reduction reactions that were considered to take place were the following:



Following elementary kinetic laws and using the experimental data from Iliuta et al., the rate for reaction r_1 was

$$r_{s1} = a_0(1 - X)k_{s1}C_{CH_4}C_{NiO}C_{Ni} \quad (8),$$

where a_0 is the initial unoxidized catalyst area, X is conversion, k_{s1} is the rate constant for reaction 1, C_{CH_4} is the concentration of CH_4 , C_{NiO} is the concentration of NiO , and C_{Ni} is the concentration of Ni , with other rates following similarly (2010). These reactions and their rates are all dependent on the concentrations of the species on the solid particle surface.

For the oxidation phase of the simulation, all of the above reduction reactions were left in place, with the addition of another single oxidation reaction. The reduction reactions were left in the code to provide a pathway for the remaining fuel to react once the feed conditions were changed from reductive to oxidative. The oxidation reaction considered to take place was the following:



The oxidation reaction rate and kinetic parameters were obtained from experimental data presented by Dueso et al. (2012). These kinetics were chosen over the oxidation kinetics presented by Iliuta et al. because of their simplicity (2010).

Previous research performed using Fluent[®] by Boudreau & Rocheleau made use of kinetics that involved partial pressures of species and coupled those pressures to mass fractions

(2010). The kinetics used for this project were solely in terms of concentrations, leading to the reworking of the previous code in order to properly define species and reactions.

3.1.2 Catalysts

Iliuta et al. used a catalyst of nickel oxide on an alumina carrier, $(\text{NiO})\text{Al}_2\text{O}_3$, to determine experimental reaction kinetics and rate laws (2010). Accordingly, the catalyst particles in the present simulations were set up to be the same, with catalyst surface area per weight taken to be as presented by Iliuta et al. (2010). The catalyst pellets used in the model were spherical particles with a density of 1700 kg/m^3 . For the reduction phase, the catalyst particles were set to have an initial oxidized fraction of 0.8 to reflect the conditions for the beginning of CLC reduction. For the oxidation phase the fraction of NiO was set to 0.2 and the fraction of Ni to 0.8 to reflect mostly reduced reactor conditions. As the reduction phase ran a decrease in the fraction of oxidized sites occurred. In the oxidation phase, oxygen bound to the reduced catalyst sites.

3.1.3 Diffusivity

In order to accurately describe the diffusion of the feed gases inside the model, multiple types of mass diffusion were taken into consideration. Molecular diffusion in the fluid phase, as well as Knudsen diffusion inside the catalyst were calculated for the present simulation using MathCAD[®]. Knudsen diffusion is the diffusion of species through a small pore in a catalyst particle, taking into account pore size and a non-linear, tortuous path. These diffusivity values were calculated using the Fuller, Schettler and Giddings correlations for binary diffusivity calculations.

3.2 Simulation Model Preliminary Steps

Several steps were taken before the actual simulation of interest was able to run. All models used needed to be scaled to an appropriate size based upon the size of the catalyst

particle. Next a periodic flow model was set up to achieve an inlet flow profile for use in the non-periodic reaction model. Finally, boundary conditions, including UDF coupled conditions, needed to be correctly established for all models.

3.2.1 Model and Geometry Scaling

The model used for the present simulations was originally developed by Nijemeisland & Dixon and included a mesh that consisted of 1,536,665 tetrahedral cells (2004). Mesh independence was determined by Nijemeisland & Dixon by comparing axial velocity components at two different mesh densities (2004). The mesh on all solid particles in the reactor wedge is shown in Figure 4 and a closer view of a central particle is shown in Figure 5.

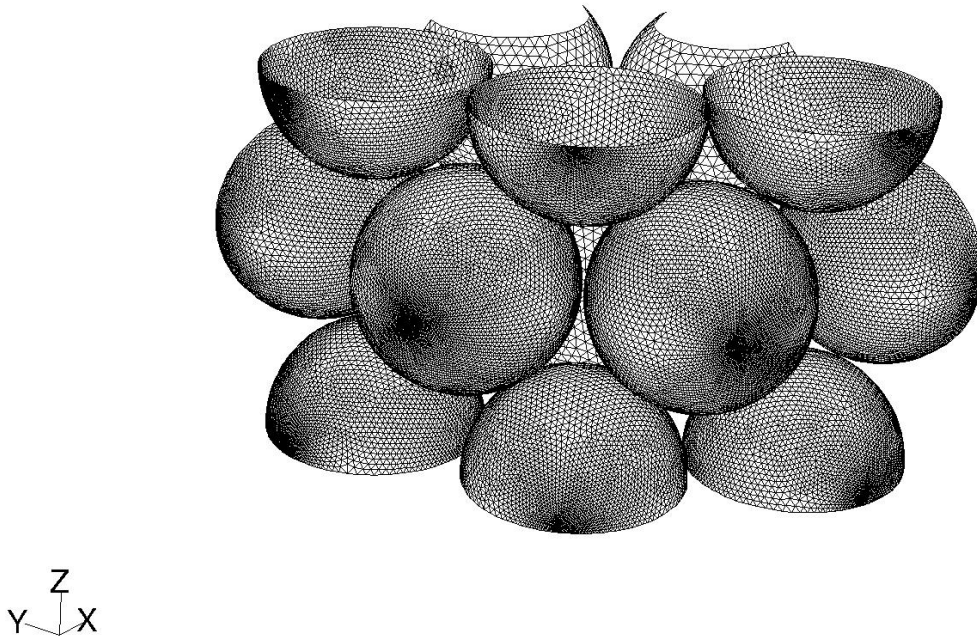


Figure 4: Particle Mesh in Reaction Model

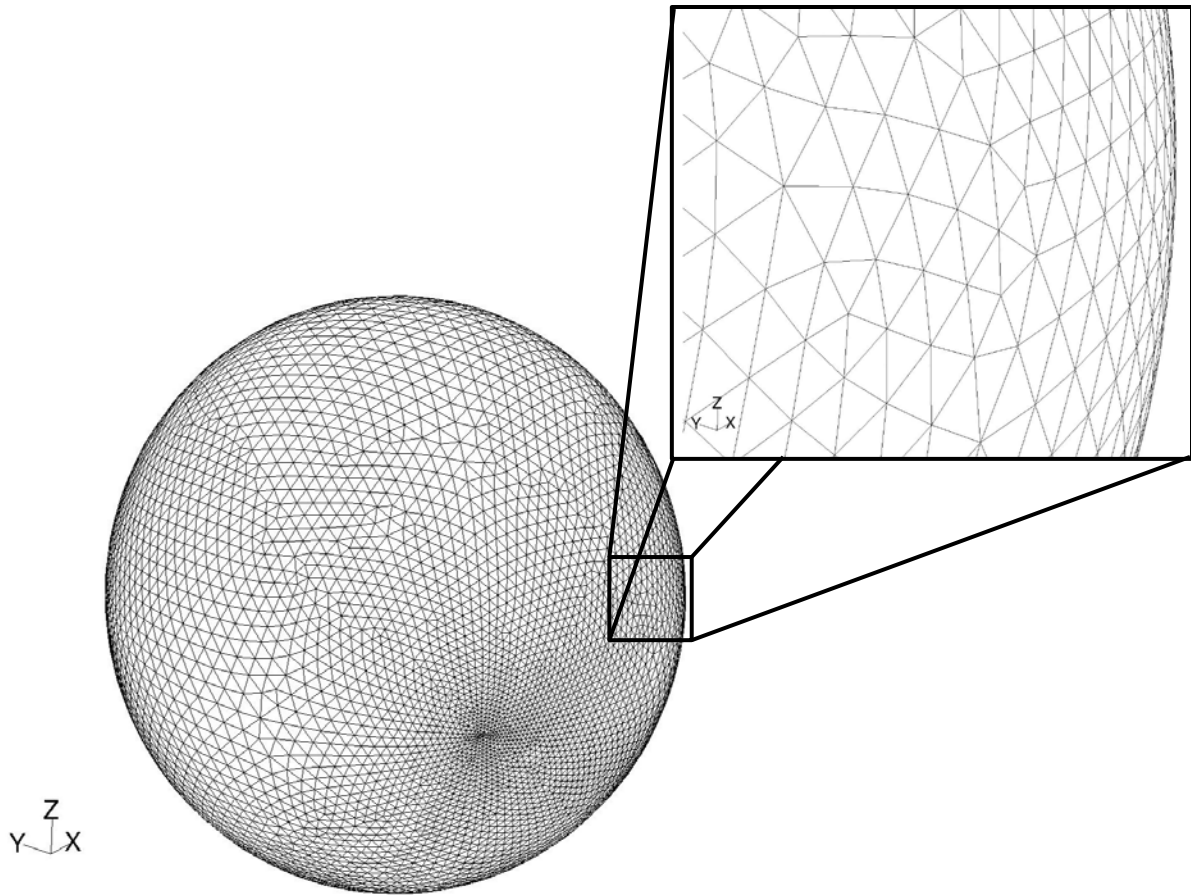


Figure 5: Single Center Particle Mesh

One of the preliminary steps required for a successful demonstration of chemical looping was to scale the existing model geometry to reflect a reasonably sized catalyst particle for CLC. The existing geometry supplied for the project depicted a one inch diameter particle in a 120° segment of a cylindrical tube with a radius of two inches, which is an unreasonably large size for a particle in CLC (Nijemeisland & Dixon, 2004). As an approximation to packed bed reactor particle sizes for CLC in industry, the model was scaled to have a particle radius of two mm and thus a cylinder radius of four mm. Additional catalyst particles were present in order to provide realistic surroundings to the main particle. The area around the main particle of concern was not meant to be an accurate representation of the reactor, but rather was intended to give a representative background for flow around the main particle. Scaling down the model was

necessary to achieve a more realistic surface area as compared to the background flow pattern for the reactions taking place.

3.2.2 Periodic Model

A fluid flow profile for the bottom (entrance) of the reaction model needed to be established. Because the model was meant to depict a small slice somewhere inside the middle of a large reactor, it was desirable to have a fully developed flow profile for the entrance. This profile represented how fluid would have been disrupted by similar particles to the modeled ones just prior to the model boundaries.

In order to get this inlet/outlet flow pattern, periodic flow settings were used in a separate simulation from the one in which looping was later simulated. The model was set up using a $k-\omega$ turbulence model, but without reactions, mass transfer, or heat effects, using a mixture of gases identical to that used in subsequent looping simulations. The mass fractions chosen for the mixture used were taken from experimental data showing concentrations as a function of time to represent a continuously fed process (Iliuta et al., 2010). The model ran until a “periodic” flow pattern was converged. This means the flow pattern into the bottom of the wedge was equal to the flow pattern out of the top. This translational periodicity was possible because the model was symmetrical vertically.

Once periodic flow was achieved for the inlet and outlet, an actual flow velocity field for the inside of the model was determined. The periodic flow model was used to write a flow profile file from the exit. A profile file contains information about any variables chosen at all points along a boundary, and can be exported from a model for subsequent use in a different model along an equally sized boundary. This profile was then read into the non-periodic reaction models and set as the inlet boundary condition. The flow field for each reaction model was then

calculated by running the non-periodic reaction models without any reactions taking place, so that flow and turbulence, along with diffusion and heat effects, were the only quantities being solved for. Reactions were not critical to this stage of the simulation and would have only increased the time the simulation would have taken to converge. Different profile files were created for the reduction and oxidation phases of looping. The inlet conditions for the reduction and oxidation models were set to mass fractions as shown in Table 2.

Table 2: Mass Fractions for Inlet Conditions

Species	Reduction Mass Fraction	Oxidation Mass Fraction
CO₂	0.028	0.001
H₂O	0.114	0.001
H₂	0.457	0
CO	0.173	0
CH₄	0.228	0
O₂	0	0.998

Values for the reduction mass fractions were chosen to represent the middle of a reactor, in the middle of a reduction cycle. Accordingly, these values were taken from gas distribution data partway through an experimental reduction cycle presented by Iliuta et al. (2010). The oxidation phase distributions were chosen to represent an almost pure oxygen feed. Fluent[®] suffered a severe error when solutions were attempted with no species present and oxygen obtained by difference. Accordingly, a small amount of CO₂ and H₂O was added to allow a solution to be obtained while still representing an almost pure oxygen feed.

The flow profile was judged to be converged after 500 iterations. Surface monitors for outlet z-direction velocity and pressure on the outlet surface were constant and residuals had dropped by two orders of magnitude, leading to this judgment.

3.2.3 Reaction Model Set Up

For each non-periodic reaction model that was used, model settings had to be carefully chosen. Boundary conditions for the walls of the reactor wedge, all sides of all particles, and the inlet and outlet needed to be set correctly. Zero flux boundary conditions were set for the cylinder walls and the cylinder surface was set to a constant temperature of 1200 K. The inlet was set to the flow profile produced from the periodic simulation, and the outlet was set to be a simple pressure outlet. Boundary conditions dealing with the interface between the solid phase and fluid phase on the particles presented the greatest challenge. The models in this project used Fluent's[®] built in species for the fluid phase but necessitated the use of User Defined Scalars (UDS) for the species within the porous solid region of the particles, creating a problem of continuity. Fluent[®] does not possess a method for determining continuity across a solid-fluid boundary where UDS are present on one side and corresponding species and UDS are present on the other. To get around this problem code was written coupling the values of the UDS in the solid phase to those of the UDS in the fluid phase.

3.2.4 Additional Model Parameters

Turbulence for the simulations was modeled using the $k - \omega$ turbulence model. This model was chosen as it was applicable to wall-bounded flows. Due to the way Fluent[®] keeps track of UDS in the mesh cells, scalar discretization settings needed to be chosen. First-order upwind discretization was used for the solution of all UDS. In first-order discretization, Fluent[®] assumes the values for a UDS, ϕ , along a face of a cell are equal to the value inside the cell upstream of that face.

In order to limit the change in any UDS Fluent[®] solved, under-relaxation factors were set. Under-relaxation factors in the pressure-based solver served to reduce the change in a UDS, ϕ , by an amount specified, according to the equation

$$\phi = \phi_{old} + \alpha\Delta\phi \quad (9)$$

where ϕ_{old} is the value of ϕ at a previous iteration, α is the under-relaxation factor, and $\Delta\phi$ is the incremental change in ϕ in an iteration.

The operating temperature of all models was chosen based on preliminary enthalpy calculations performed to ensure favorable conditions for the reactions considered. Reaction enthalpy changes were calculated as shown in Appendix B.

3.3 User Defined Scalars and Functions

User defined functions were coded to reflect the chosen kinetics and operating conditions. These functions included code that coupled the user defined scalars that represented the concentrations of species to the mass fractions used by Fluent[®], source terms for all species present in all phases, reaction heat terms, and diffusivity definitions. To track how a UDS changes with time, Fluent[®] solves the transport equation

$$\frac{\partial \rho \phi_k}{\partial t} + \frac{\partial}{\partial x_i} \left(\rho u_i \phi_k - \Gamma_k \frac{\partial \phi_k}{\partial x_i} \right) = S_{\phi_k} \quad k = 1, \dots, N \quad (10)$$

for an arbitrary UDS, ϕ_k , where u_i is the velocity of the fluid phase, Γ_k is the diffusion coefficient for the UDS, and S_{ϕ_k} is the source term for the UDS (UDS Theory, 2006).

Source terms were coded for four species that were present in all phases, and three species present in the solid phase only. The source term for the UDS corresponding to H_2 was of the form

$$S_{H_2} = \rho_s * \left(\sum_{i=1}^4 \alpha_{i,H_2} r_{si} \right) * MW_{H_2} \quad (11)$$

where i is the reaction number, α is the stoichiometric coefficient of H_2 in reaction i , and MW_{H_2} is the molecular weight of H_2 . Other source terms were similarly defined. In order for

Fluent[®] to solve any supplied UDS, the derivative of the UDS source with respect to the scalar must be supplied. A derivative supplied as a non-zero $\partial S/\partial \phi$ increases stability of the solution. Derivatives of each reaction rate with respect to each species concentration were obtained, and were of the form

$$dS = \rho_s * MW_{H_2} * \left(\sum_{i=1}^4 \alpha_{i,H_2} \frac{\partial r_{si}}{\partial C_{H_2}} \right) * \frac{\partial C_{H_2}}{\partial Y_{H_2}} \quad (12),$$

where the partial derivative $\frac{\partial r_{si}}{\partial C_{H_2}}$ is of the form

$$\frac{\partial r_{s2}}{\partial C_{H_2}} = a_0(1 - X) * k_{s2} C_{NiO} \quad (13),$$

and $\frac{\partial C_{H_2}}{\partial Y_{H_2}}$ is the change in concentration of H₂ with the change in mass fraction of H₂, Y_{H_2} , and is of the form

$$\frac{\partial C_{H_2}}{\partial Y_{H_2}} = \frac{\overline{MW}}{MW_{H_2}} * \frac{P}{RT} * \left(1 - Y_{H_2} \frac{\overline{MW}}{MW_{H_2}} \right) \quad (14)$$

where \overline{MW} is the average molecular weight of the fluid phase.

The species present in all phases were CO, CO₂, H₂, and H₂O. In the reduction model CH₄ was not defined as a source term, with the concentration of this species being obtained by difference. CH₄ was present in high amounts in the reduction model, therefore decreasing the required computing power if not directly calculated. In the oxidation model O₂ was obtained by difference, with all remaining species present besides CO₂ and H₂O assumed to become negligible compared to the amount of oxygen present.

The three quantities present in the solid phase only were the solid species Ni, NiO, and the conversion of Ni to NiO: X. These quantities were chosen to be modeled as species in order to keep track of surface sites available for reactions to take place, as kinetics were dependent on

the concentration of Ni and NiO. A method for keeping track of available surface sites and amount converted that was briefly considered was a feature in Fluent[®] called User Defined Memory (UDM). A set of UDM could have been defined as the number of surface sites available, and that UDM could have then been continuously updated based on the rates of diffusion and reaction. After consideration this method was rejected as it was considered to be more difficult.

The UDS used for the three solid-only species were essentially coded as if they were regular species, with the exceptions that they were not defined in the fluid phase, and they had no diffusion out of the solid phase. Zero-flux conditions were enforced for these species across phase boundaries to prevent non-real situations from forming in the model.

3.4 Transient Modeling

The main difference between this project and previous research is the inclusion of transience instead of a focus on steady state solutions. The unsteady nature of chemical looping reactors lends itself to a transient model. Solving unsteady equations in Fluent[®] requires supplying information about the unsteady solution method desired. Fluent[®] attempts to find a solution iteratively, using a number of iterations per time step set by the user. The number of iterations per time step was set to 10. It was found that using additional iterations did not advance a solution further than achieved with only 10. Correctly choosing the size for the time steps was a point of concern. Time steps that were too large caused errors in the simulation. This occurred because as Fluent[®] tried to step a solution forward in time by a large jump, error was introduced and the solution diverged. At the beginning of the simulations, small time steps were used, beginning with $1 * 10^{-6}$ seconds, and the step size was increased by powers of 10 as the simulations progressed.

A larger time step is desired in order to observe a larger period of the looping cycle. If time steps of $1 * 10^{-6}$ seconds were used for the entirety of the simulation period, very little overall time would elapse. This would limit the collection of detailed data about the reactions taking place.

3.5 Reduction Phase Reaction Model

For the reduction phase reaction model, the mass fraction of oxidized catalyst sites was set to 0.8 and the un-oxidized fraction to 0.2. These values were chosen to reflect a highly oxidized starting point for the reduction phase. Conversion was initially set to 0.5 to allow room to show change in conversion over time. Surface monitors were set up to keep track of variables such as temperature, pressure, and UDS mass fractions on particle surfaces to aid in judging convergence or divergence of the model. After preliminary iterations, the reduction phase was run isothermally to achieve a more stable solution. Data files were written every two time steps to show transient changes in model variables.

3.5.1 Bootstrapping

Initially, the reduction reaction model was set to run with only the equations for flow, energy, and turbulence being solved. This was at first “primed” by running at steady state for several hundred iterations, before a transient solution method was adopted. After this change, equations were added to the solver for all of the UDS present in the solid phase, Ni, NiO, and X, along with the equations for one of the multi-phase UDSs. This was performed in this manner because all of the UDS source terms depended on the concentrations of Ni, NiO, and the reaction conversion, X. When these equations were initially added changes were made to the code to artificially reduce all of the reaction rates to 1% of their actual value. This was performed to negate any potential divergence from suddenly adding rapid reactions into the model. Once this

was running stable at unsteady state using time steps of 10^{-6} seconds, more UDS source equations were added, one at a time. As the model progressed, attempts were made to increase the reaction rates.

3.6 Oxidation Phase Reaction Model

For the oxidation phase reaction model, the mass fraction of oxidized catalyst sites was set to 0.2 and the un-oxidized fraction to 0.8. These values were chosen to reflect a highly reduced starting point for the oxidation phase. Conversion was initially set to 0.5 to allow room to show change in conversion over time. Surface monitors were set up to keep track of variables such as temperature, pressure, and UDS mass fractions on particle surfaces to aid in judging convergence or divergence of the model. Data files were written every time step to show transient changes in model variables.

3.6.1 Bootstrapping

Initially, the oxidation reaction model was set to run with only the equations for flow, energy, and turbulence being solved. Next, equations were added to the solver for each species and the corresponding UDS, one at a time. This was performed in this manner because the solution became unstable when all equations were solved simultaneously. When these equations were initially added, changes were made to the code to artificially reduce all of the reaction rates to 1% of their actual value. This was performed to negate any potential divergence when suddenly adding rapid reactions into the model. Once this was running stable at unsteady state using time steps of 10^{-6} seconds, the size of the time step was gradually increased.

4. Results and Discussion

A periodic flow model was solved and was judged to be converged. A flow profile from the periodic simulation was used to provide inlet flow information for subsequent non-periodic simulations. Data was collected for both the reduction and oxidation phases of looping. Transient changes in species and other parameters were observed. Trends obtained for both phases of looping are presented. Qualitative comparisons to experimentally obtained trends were made. For all data shown below, two central particles and one half particle were used. The half particle was included to provide example results for the surroundings of the central particles. The location of these particles within the model is shown in Figure 6. Fluent[®] 14.0 was used for post processing.

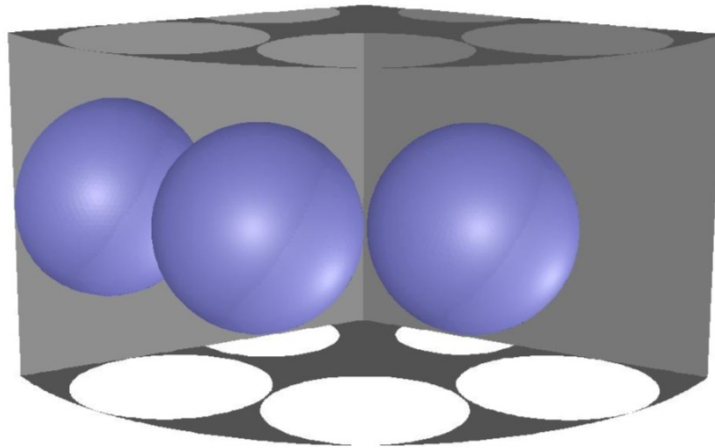


Figure 6: Location of Central Particles

4.1 Periodic Flow

The periodic model was judged to have converged by the observation of residuals between iterative solutions, and surface monitors. The model was allowed to run for 500 iterations. The residuals for this model are shown in Figure 7.

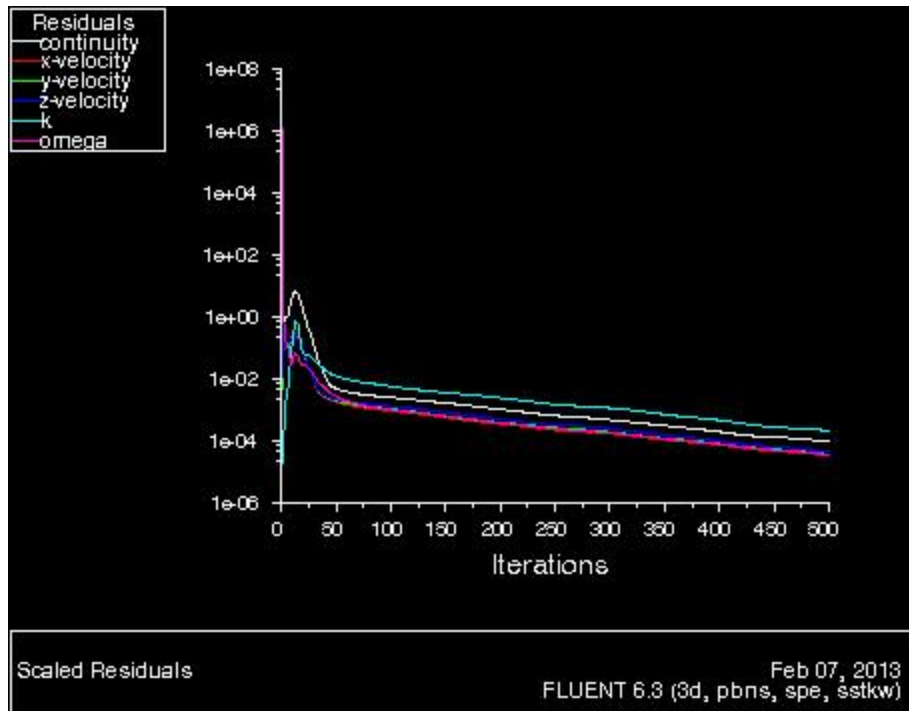


Figure 7: Periodic Flow Model Solution Residuals

The residuals dropped over two orders of magnitude during the 500 iterations. This drop coupled with the constant surface monitors allowed us to claim convergence of the model.

Surface monitors were created to keep track of integral values of pressure and z-direction velocity on the translational periodic boundary to assist in tracking model convergence. After less than a hundred iterations the surface monitors appeared totally constant, and continued to remain so. Only the first 150 iterations are presented as they continued the trend after this point. The monitors for pressure and z-direction velocity are shown below in Figure 8 and Figure 9 respectively.

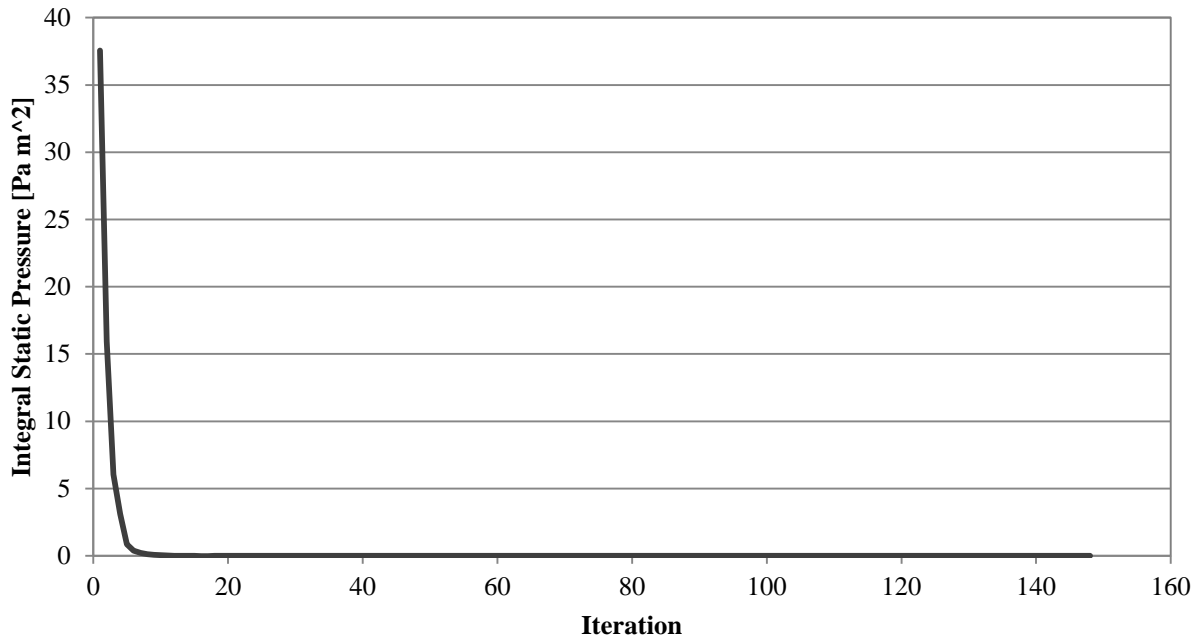


Figure 8: Convergence History of Static Pressure on top

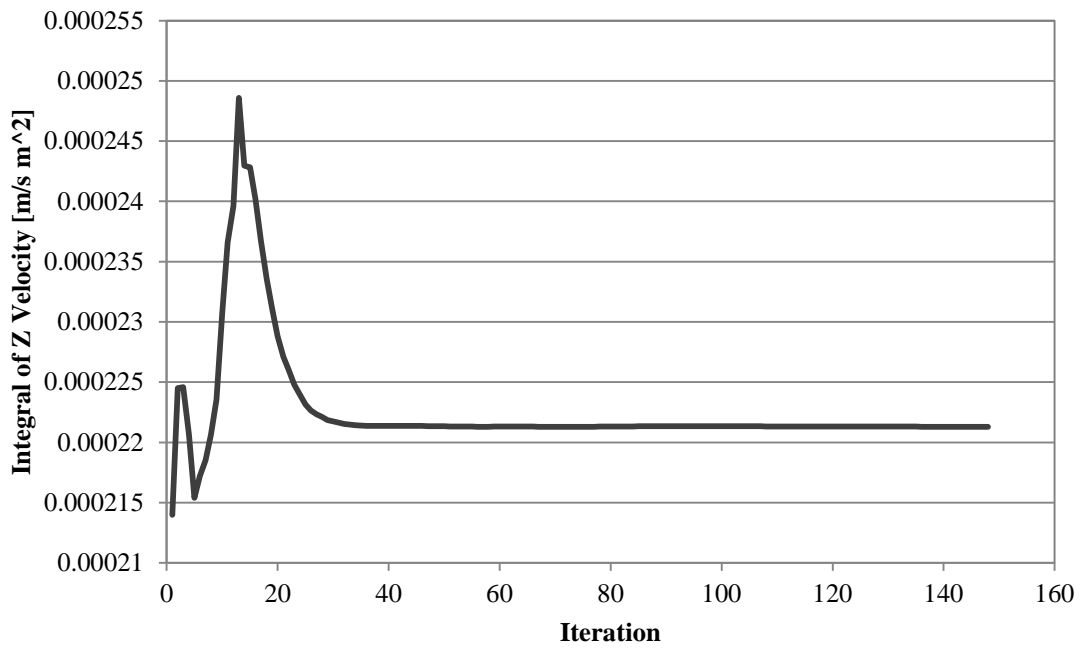


Figure 9: Convergence History of Z Velocity on top

After convergence was achieved, a flow profile file was written and used in the subsequent reduction model for inlet flow conditions. This periodic model was re-run with different conditions to obtain a profile file for the oxidation model.

4.2 Reduction Phase

Reduction data was collected with all UDS equations solved simultaneously, along with turbulence, energy, and flow equations. Time steps of $1 * 10^{-6}$ seconds each were used initially. After these step sizes were successful, they were gradually increased up to a maximum of 0.1 seconds. At this point the simulation was unstable and errors were frequent. To attempt to stabilize the solutions obtained, the model was run isothermally with time steps of $1 * 10^{-4}$ seconds. This led to better data collection for most of the desired parameters. Running the model isothermally prevented UDS sources for Ni, NiO, and X from changing, due to their temperature dependence. Isothermal simulation provided transient changes in all other species and quantities of interest, and was primarily used for data collection.

As shown by Iliuta et al., as the reduction phase progressed a consumption of methane should be observed along with production of CO₂ and H₂O (2010). This was observed across the central particles of focus in the model. Methane mass fractions at the beginning and end of the isothermal simulation are shown in Figure 10 and Figure 11. The time elapsed between these and subsequent pairs of images was $8 * 10^{-4}$ seconds. These figures show a consumption of methane with time.

The increase of the combustion products CO₂ and H₂O was observed across the three central particles. The change in mass fractions of CO₂ with time is shown in Figure 12 and Figure 13.

The change in mass fractions of H₂O is shown in Figure 14 and Figure 15.

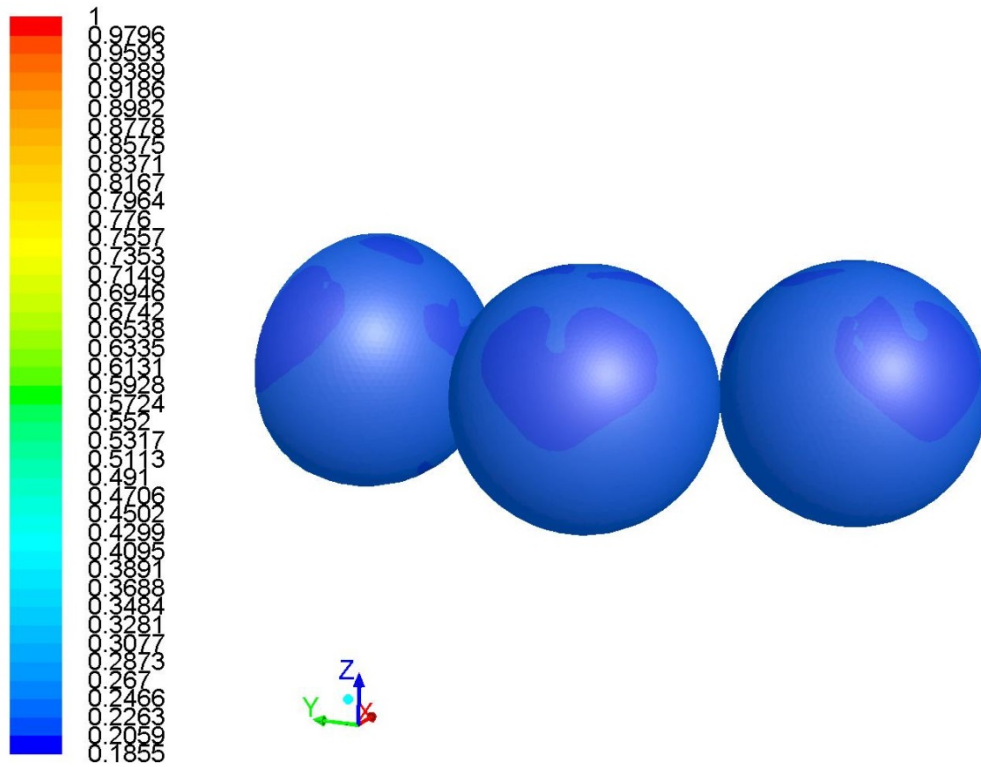


Figure 10: Contour of Mass Fraction of CH₄ on Central Particles (Time = 1.48E-3)

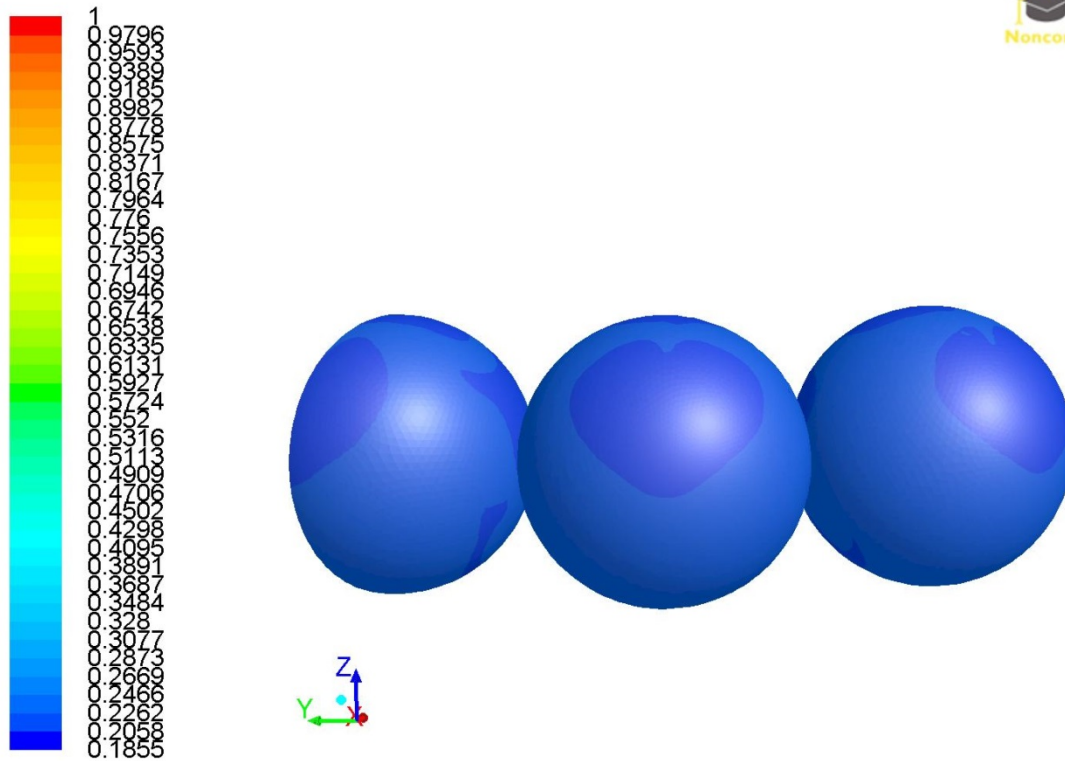


Figure 11: Contours of Mass Fractions of CH₄ on Central Particles (Time = 2.28E-3)

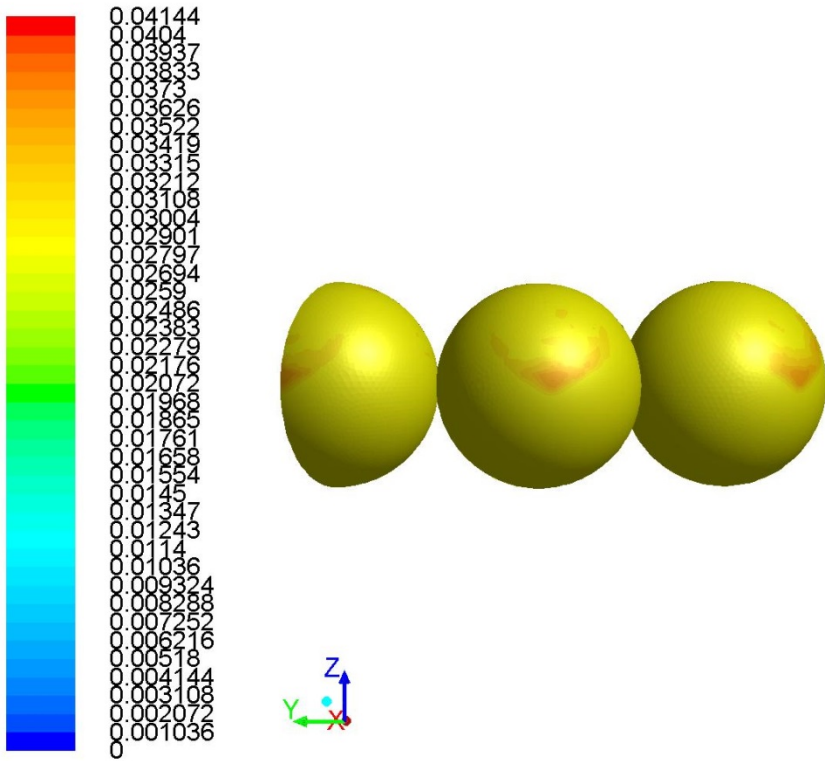


Figure 12: Contours of Mass Fractions of CO₂ on Central Particles (Time = 1.48E-3)

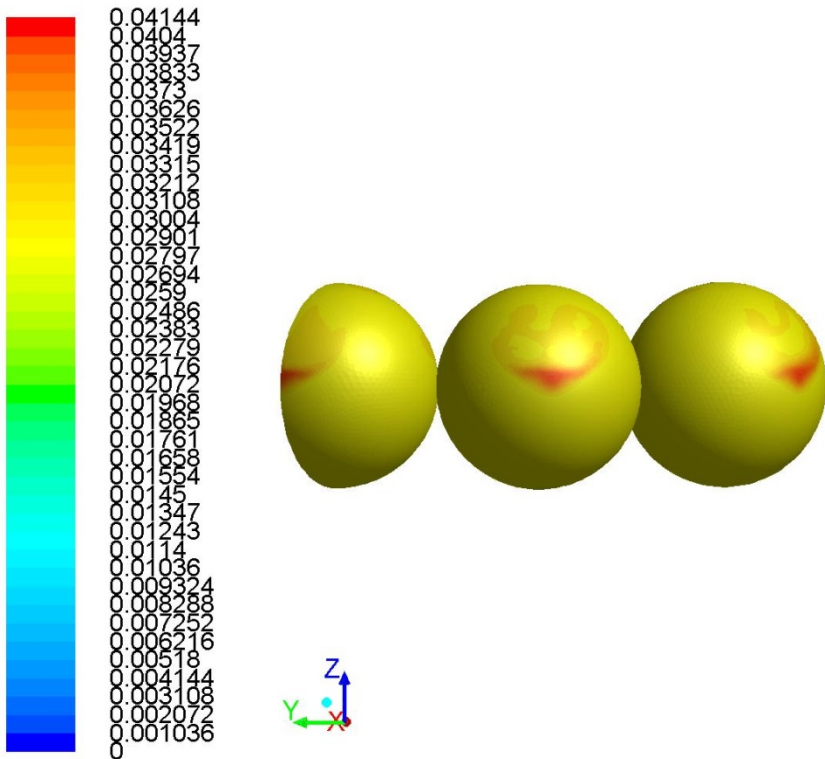


Figure 13: Contours of Mass Fractions of CO₂ on Central Particles (Time = 2.28E-3)

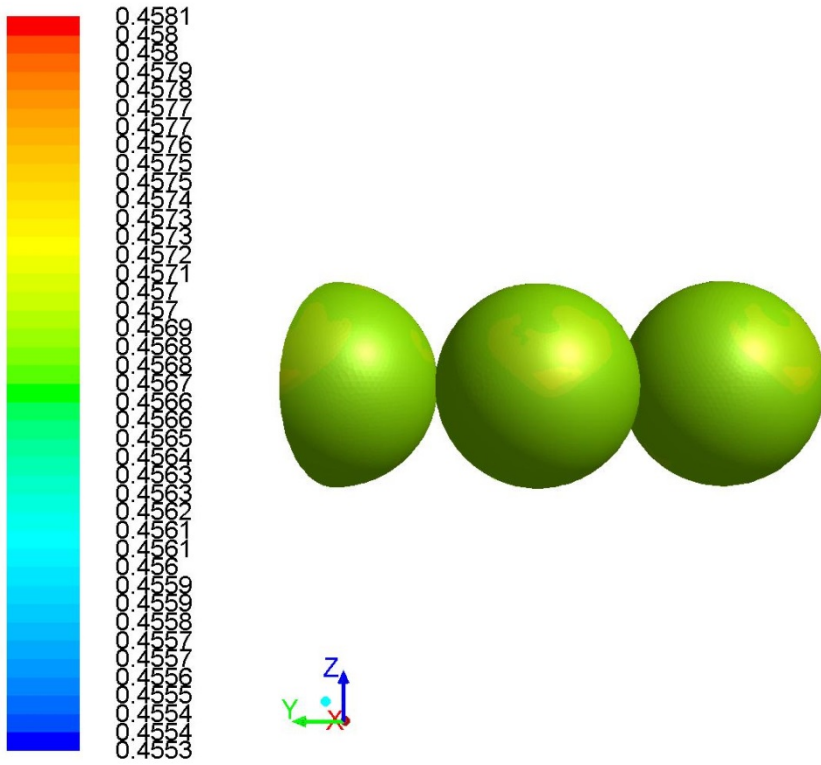


Figure 14: Contours of Scalar-1: Mass Fractions of H₂O on Central Particles (Time = 1.48E-3)

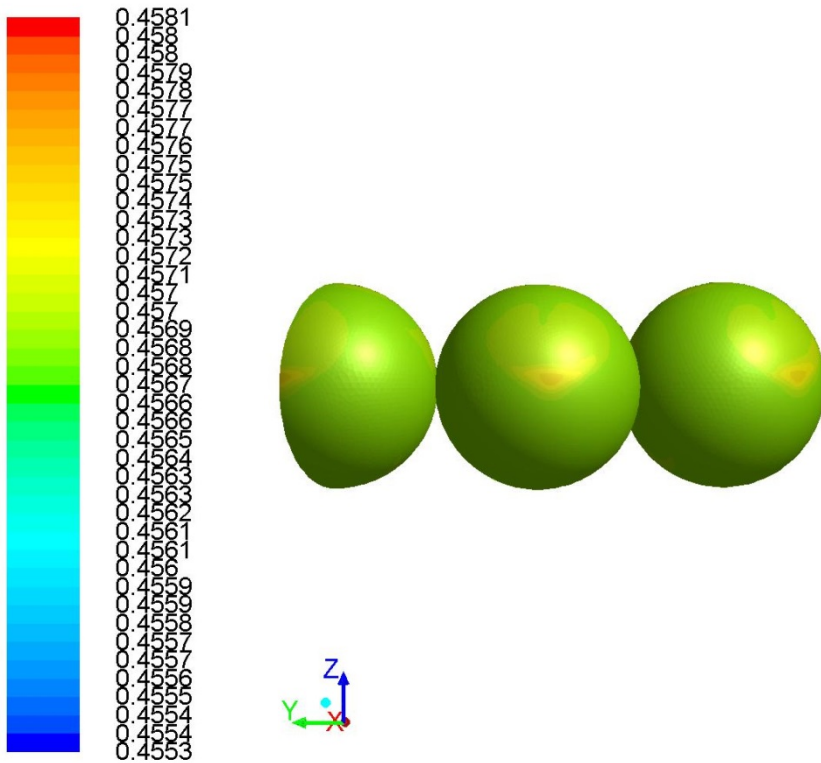


Figure 15: Contours of Scalar-1: Mass Fractions of H₂O on Central Particles (Time = 2.28E-3)

The demonstrated increase in these combustion products, coupled with the decrease in methane indicates qualitative expectations were met for the reduction phase of looping. The actual quantitative values of each species are not accurate, but such an accurate comparison was not the goal of this simulation.

The concentration of Ni did not change over time within the isothermal simulation. This was due to the temperature dependence of terms in the Ni source. Isothermal values of the Ni concentrations varied along the surface of the particle, shown in Figure 16. The highest concentrations on the upper portion of the particles below coincide with the location of temperature hotspots, shown in Figure 17. These hotspots are due to the proximity of the cylinder wall, held at 1200 K, to the particles.

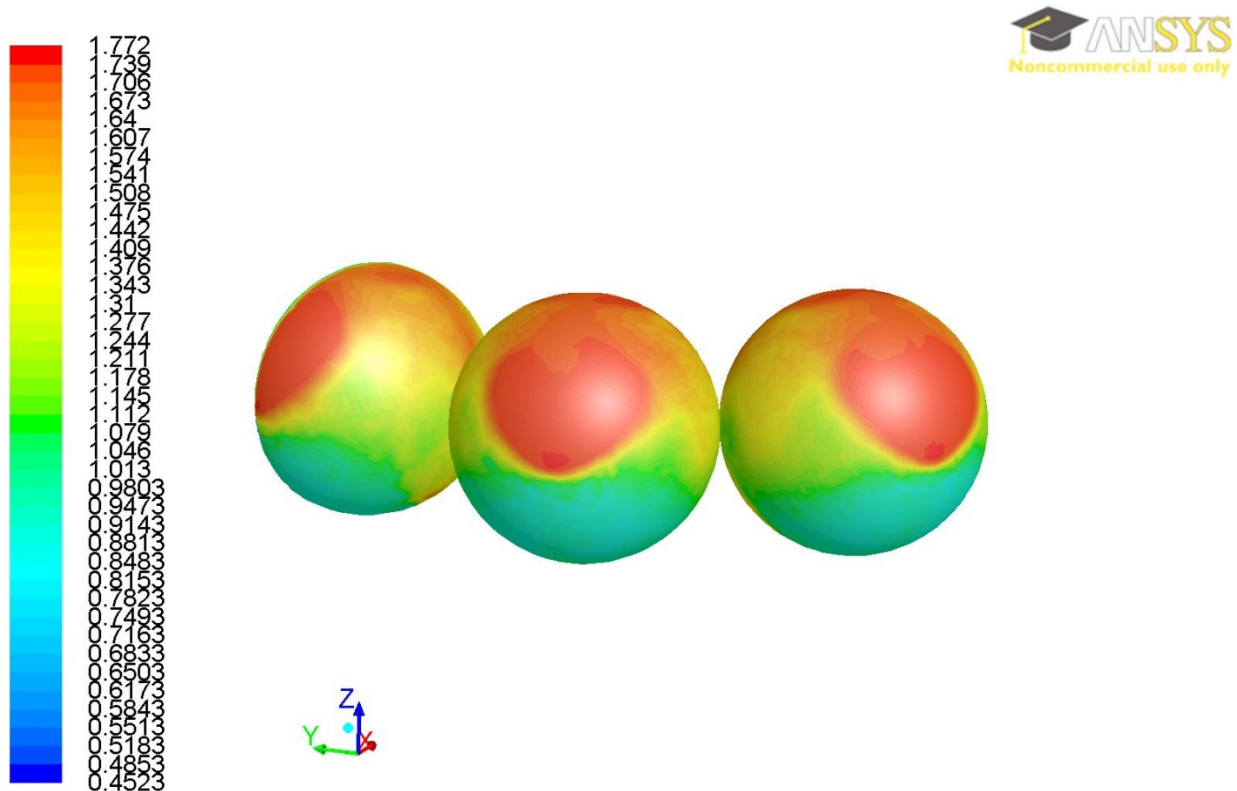


Figure 16: Contours of Scalar-5: Concentrations of Ni on Central Particles (Time = 1.48E-3)

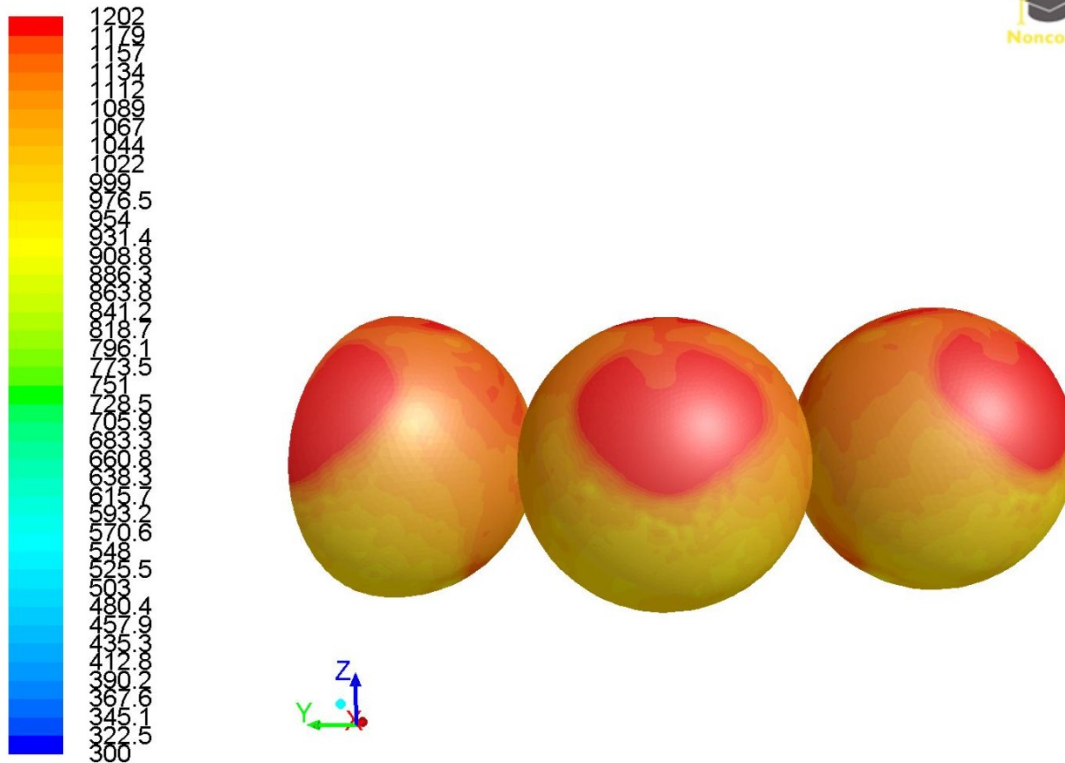


Figure 17: Contours of Static Temperature [K] on Central Particles (Time = 1.88E-3)

For comparison, data from before the simulation was run isothermally is provided in Figure 18. The locations of high and low concentrations along the particle are similar to those observed in the isothermally collected data, but the numerical values are lower. This shows that in non-isothermal operation these values did change.

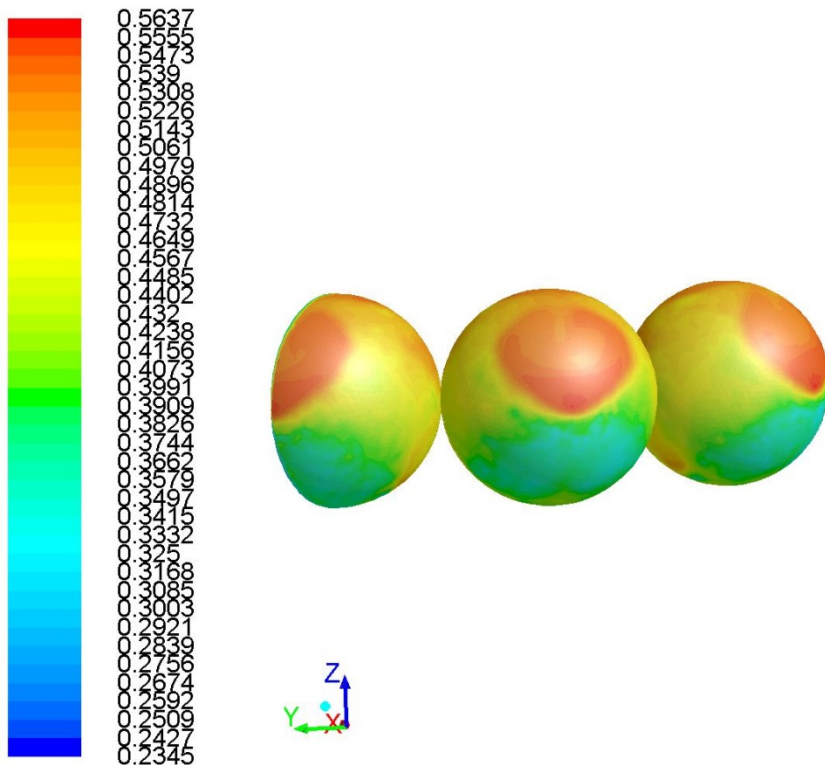


Figure 18: Contours of Scalar-5: Non-isothermal Concentrations of Ni on Central Particles (Time = 2.28E-3)

4.3 Oxidation Phase

Oxidation phase data was collected with all UDS equations solved simultaneously, along with turbulence, energy, and flow equations. Time steps of $1 * 10^{-6}$ seconds each were used initially. After these step sizes were successful, they were gradually increased up to a maximum of $1 * 10^{-3}$. At this point the simulation was stable. Time steps of $1 * 10^{-2}$ were attempted but the simulation became unstable. The oxidation reaction taking place was generally considered to be slower than the reduction phase reactions. This slower rate of reaction could have contributed to the increased stability of the larger time steps as compared to the reduction phase.

To show a qualitatively successful oxidation phase, the concentration of Ni was expected to decrease and NiO to increase, as the catalyst was oxidized. This was observed across the central particles of focus in the model. The change in Ni concentrations at the beginning and end of a period of $8 * 10^{-3}$ seconds is shown in Figure 19 and Figure 20 respectively.

The locations of high and low concentrations of Ni on the particle remained similar over time, but the scale changed enough to show definite oxidation of Ni sites taking place.

As the concentrations of Ni on the catalyst particles decreased, it was expected that the concentrations of NiO would increase. This was observed, and is shown at the beginning and end of a period of 8×10^{-3} seconds in Figure 21 and Figure 22 respectively.

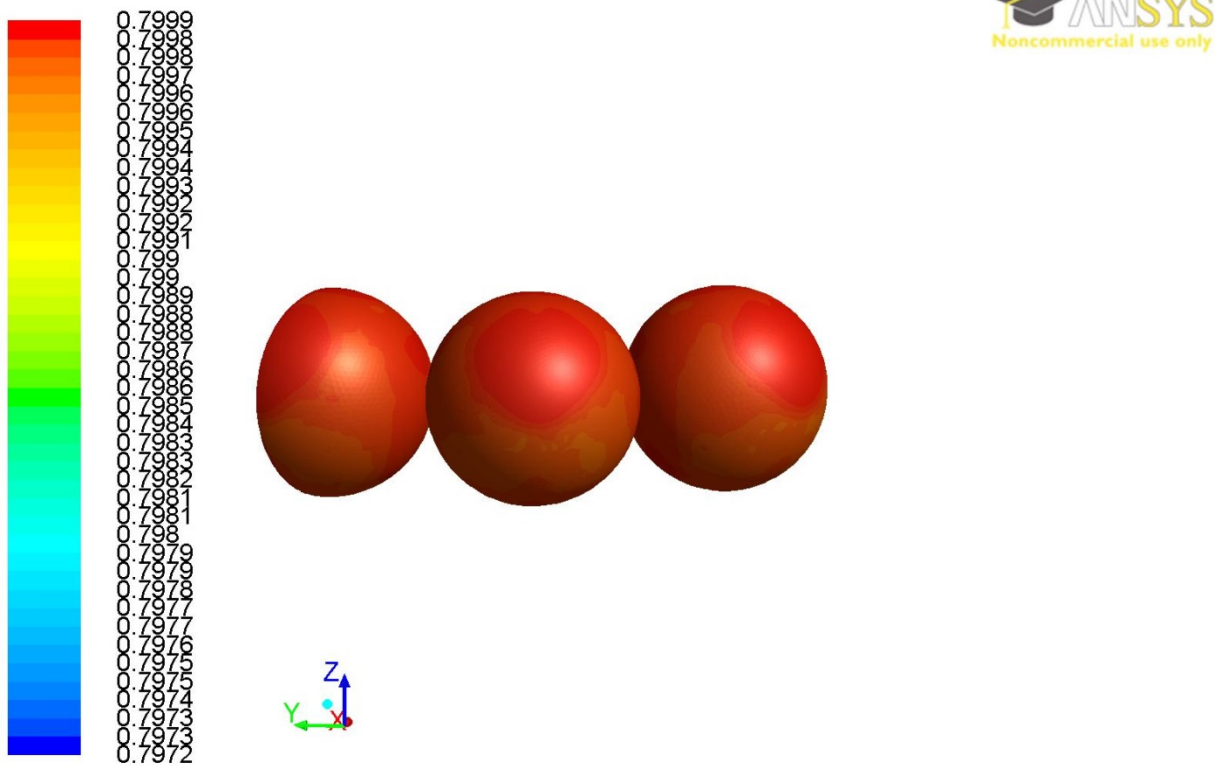


Figure 19: Contours of Scalar-5: Concentrations of Ni on Central Particles (Time = 9.23E-3)

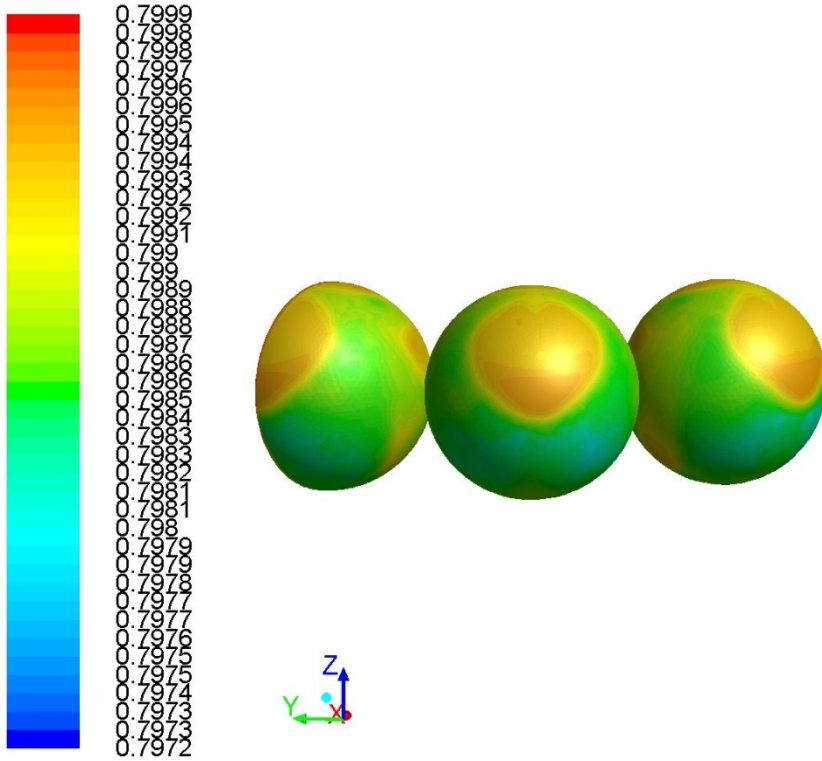


Figure 20: Contours of Scalar-5: Concentrations of Ni on Central Particles (Time = 1.723E-2)

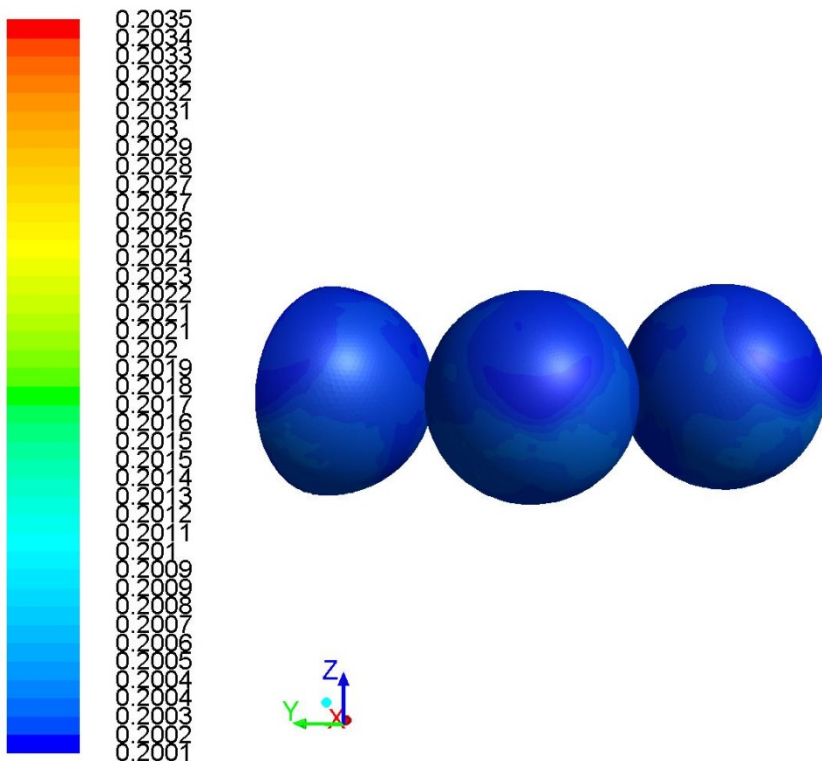


Figure 21: Contours of Scalar-6: Concentrations of NiO on Central Particles (Time = 9.23E-3)

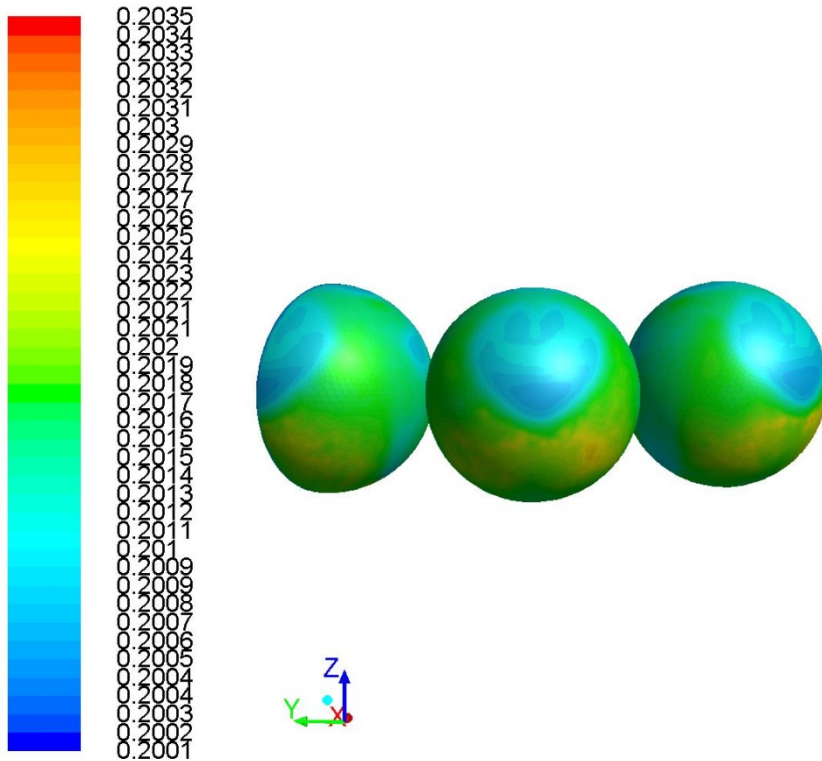


Figure 22: Contours of Scalar-6: Concentrations of NiO on Central Particles (Time = 1.723E-2)

The amount of NiO on the catalyst particle increased over time. The particles showed the most dramatic increase was towards the bottom of the particle, nearest to the inlet of reacting gas. This was as expected, since the oxygen would be expected to react with those sites first.

Temperature across the central particles was monitored and decreased as time elapsed, as expected. This was predicted due to the endothermic nature of the oxidation reaction taking place, shown by preliminary enthalpy calculations performed, as shown in Appendix B.

Temperature changes across the central particles at the beginning and end of a period of time of $8 * 10^{-3}$ seconds are shown in Figure 23 and Figure 24 respectively.

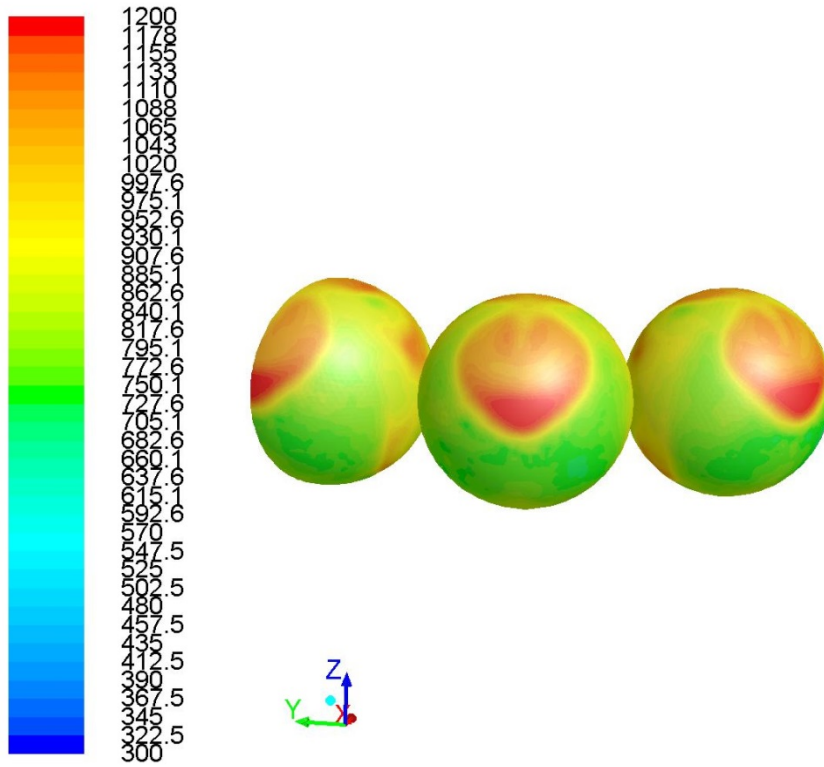


Figure 23: Contours of Static Temperature [K] on Central Particles (Time = 9.23×10^{-3})

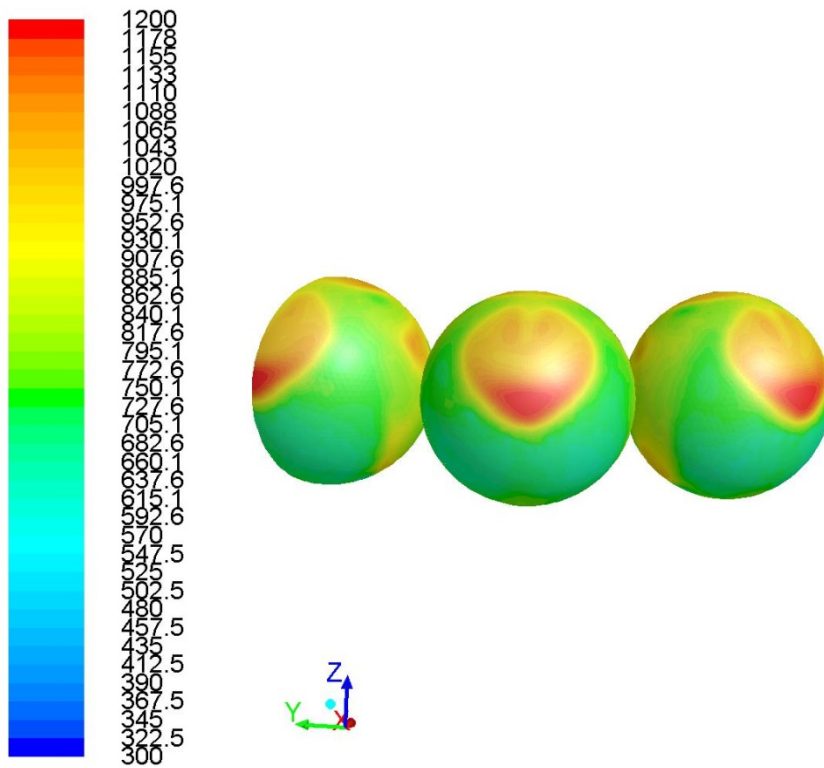


Figure 24: Contours of Static Temperature [K] on Central Particles (Time = 1.723×10^{-2})

The temperatures on the particles were lowest towards the bottom of the particles, nearest the incoming reacting gas. The hot spots shown on the upper side of each particle are present due to the proximity of the cylinder wall, held at 1200 K. The temperature was shown to decrease most in areas of high oxidation.

5. Conclusions and Recommendations

From the data gathered in the simulations of both the reduction and oxidation phases, it was determined that transient simulation of CLC using CFD is possible. This section presents the conclusions of the project, along with possible further avenues of research.

5.1 Feasibility of CFD simulation of transient reactions.

The reduction phase of looping demonstrated the expected qualitative results. Accurate quantitative results were not obtained, as expected. Isothermal simulation aided in stabilizing the solution of many quantities, but prevented the demonstration of transient changes in the solid quantities Ni, NiO, and X.

From the difficulties encountered throughout this project, it is likely impossible to simulate both reduction and oxidation phases of CLC autonomously within the same model with the current technology. There appears to be no viable method to automatically switch inlet flow conditions.

Thus, computational fluid dynamics software can be used to simulate transient chemical reactions, as illustrated with this example of chemical looping combustion. However, a full, realistically accurate simulation is not easily possible although results display expected qualitative trends.

5.2 Future Research

Within the framework of the Fluent[®] software package, multiple possibilities for future research exist. Attempting the same simulations with larger time steps and full reaction rates would be recommended. Computing power is a limiting factor for such simulations. Attempting non-isothermal simulation of the reduction phase of CLC is another recommendation.

The simulation of different reactions would provide valuable data. Using either different experimentally obtained reaction kinetics, or using an entirely different looping reaction set, such as Chemical Looping Reforming (CLR) would provide useful data.

Exploring the use of alternate software packages such as COMSOL, or Fluent[®] 14.0 may provide better results than those obtained using Fluent[®] 6.3.26. Alternatively, it may be found that those packages are not as effective.

An avenue of future research that could yield valuable results would be to simulate a new geometry with a larger tube to particle diameter ratio. This would allow more full particles to be simulated, and would reduce the effects of the proximity of the cylinder wall. Computing power would be a limiting factor in such a simulation.

Based on the research experiences of this project it is predicted that simulation of a single dual-phase model that would switch automatically between phases is impossible. There is no viable method to automatically change the inlet flow conditions partway through a simulation, with the present software.

6. Nomenclature

a_0 = initial particle unoxidized area, m^2/kg_{carrier}
 C = concentration, kg/m^3 or lb_m/ft^3 or kg/kg_{carrier}
 D = diffusivity m^2/s or ft^2/s
 J = diffusive flux, $kmol/m^2s$ or kg/m^2s or lb_m/ft^2s
 k = reaction rate constant, units vary
 m = stoichiometric coefficient
 MW = molecular weight, $kg/kmol$ or $lb_m/lbmol$
 \overline{MW} = average molecular weight
 n = stoichiometric coefficient
 r = reaction rate, $kmol/kg\ s$
 R = rate of production, $kmol/m^2s$ or kg/m^2s or lb_m/ft^2s
 S = source term, $kmol/m^2s$ or kg/m^2s or lb_m/ft^2s
 Sc = Schmidt Number, $\frac{\mu}{\rho D}$
 t = time, s
 u = velocity, m/s or ft/s
 X = conversion
 Y = mass fraction

Greek Letters

α = under-relaxation factor; stoichiometric coefficient
 Γ = diffusion coefficient $kg/m\ s$
 ϕ = user defined scalar
 μ = turbulent viscosity, $Pa\ s$ or $N\ m/s$ or $lb_f\ ft/s$
 ρ = density, lb_m/ft^3 or kg/m^3

Subscript

i = species i ; reaction i
 j = species j
 k = user defined variable number
 m = mixture m
 x = number of atoms of a component in chemical compound; Number of metal atoms in a metal oxide
 y = number of oxygen atoms in a metal oxide; $y-1$ = Number of oxygen atoms - 1

Abbreviations

CFD = computational fluid dynamics

CLC = chemical looping combustion

UDF = user defined function

UDS = user defined scalar

Chemical Formulas

Al_2O_3 = alumina

CO = carbon monoxide

CO_2 = carbon dioxide

Cu = copper

Fe = iron

Fe_3O_4 = iron (III) oxide

H_2O = water

Me = metal, arbitrary

MeO = metal oxide, arbitrary

Me_xO_y = metal oxide, arbitrary

MnO = manganese (II) oxide

Ni = nickel

NiO = nickel oxide

NO_x = nitrogen oxides

TiO_2 = titanium dioxide

ZrO_2 = zirconium dioxide

7. References

- Boudreau, J.; Rocheleau, A. Comparison of catalyst geometries using computational fluid dynamics for methane steam reforming. Major Qualifying Project, Worcester Polytechnic Institute, Worcester, MA, April 2010.
- Dixon, A. G.; Taskin, M. E.; Nijemeisland, M.; Stitt, E. H. CFD method to couple three-dimensional transport and reaction inside catalyst particles to the fixed bed flow field. *Ind. Eng. Chem. Res.* **2010**, *49*, 9012-9025.
- Dueso, C.; Ortiz, M.; Abad, A.; Garcia-Labiano, F.; de Diego, L. F.; Gayan, P.; Adanez, J. Reduction and oxidation kinetics of nickel-based oxygen carriers for chemical-looping combustion and chemical-looping reforming. *Chem. Eng. J.* **2012**, *188*, 142-154.
- Fan, L.; Li, F. Chemical looping technology and its fossil energy conversion applications. *Ind. Chem. Res.* **2010**, *49*, 10200-10211.
- G8+5 Academies' joint statement: Climate change and the transformation of energy technologies for a low carbon future, 2009. The National Academics. <http://www.nationalacademies.org/includes/G8+5energy-climate09.pdf> (accessed Oct 27, 2012).
- Iliuta, I.; Tahoces, R.; Patience, G. S.; Riffart, S.; Luck, F. Chemical-looping combustion process: Kinetics and mathematical modeling. *AIChE J.* **2010**, *56*, 1063-1079.
- Lawrence Livermore National Laboratory. Estimated US Energy Use in 2011: ~97.3 Quads, 2012. Energy Flow. https://flowcharts.llnl.gov/content/energy/energy_archive/energy_flow_2011/LLNLUSEnergy2011.png (accessed Oct 25, 2012).
- Nijemeisland, M; Dixon, A. G. CFD study of fluid flow and wall heat transfer in a fixed bed of spheres. *AIChE J.* **2004**, *50*, 906-921.

Noorman, S.; van Sint Annaland, M.; Kuipers, H. Packed bed reactor technology for chemical-looping combustion. *Ind. Eng. Chem. Res.* **2007**, *46*, 4212-4220.

UDS Theory. *FLUENT 6.3 User's Guide*. Fluent Inc. 2006.

Wendt, J. F. Basic philosophy of CFD. In *Computational fluid dynamics*, Third Edition; Springer: Berlin, 2009, 3-14.

Zikanov, O. What is CFD?. In *Essential computational fluid dynamics*, John Wiley & Sons, Inc.: Hoboken, NJ, 2010.

Appendix A: Methane Reforming as a Novel Application of Chemical Looping

One improving technology in the transportation field is the fuel cell. Although there are several types, the proton exchange membrane (PEM) fuel cell offers the best opportunities for transportation. PEM fuel cells use hydrogen and air, or oxygen, as fuel to produce electricity and water. These fuel cells run at a lower temperature and are smaller than other types, making them good candidates for vehicle use. However the largest burdens are the storage and production of hydrogen gas.

Hydrogen can be produced through a variety of methods including steam reforming, partial oxidation of fossil fuels, syngas conversion, and water splitting through various means. The most common industrial method for production is steam reforming. Steam reforming is a method for producing hydrogen from hydrocarbons. Typically this fuel is natural gas, which is mostly methane. Steam methane reforming (SMR) is the predominant method for producing hydrogen in industry. Typically SMR reactions are carried out in catalytic reactors that use nickel oxide supported in alumina as the catalyst (El-Bousiffi & Gunn, 2007). Three predominant reactions are present in the reactor (Oliveira et al., 2010):



These reactors are operated at high temperatures, between 600 and 900°C, to obtain greater yield from the endothermic reactions (El-Bousiffi & Gunn, 2007; Oliveira et al., 2010).

Traditional SMR processes offer several areas for improved optimization, especially in regards energy usage. The SMR process uses a furnace provide the necessary heat to the

reformer (Molburg & Doctor, 2003). Figure A.1 shows a high level of heat integration and recycle within the process.

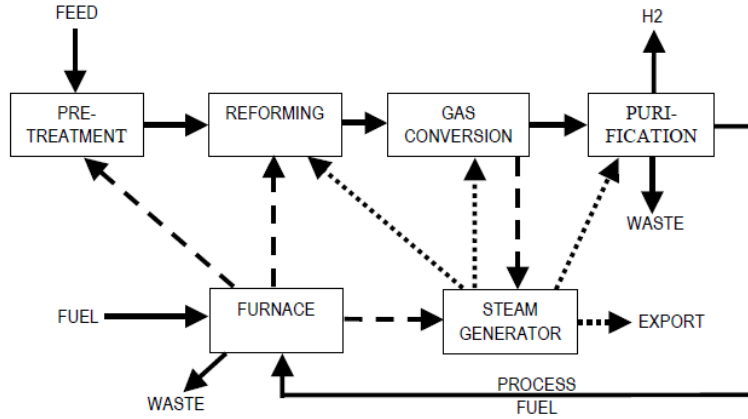
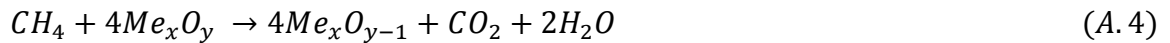


Figure A.1: SMR Process Block Diagram (Molburg & Doctor, 2003)

Ideally, in terms of environmental impact, this process should be run at the minimum temperature that can produce conversion with maximum heat integration to minimize heat waste to the environment. In practice there will be energy waste. As the demand for hydrogen is perceived to grow alternatives to the SMR process will be investigated. One current technology that offers an alternative is chemical looping.

Chemical looping reforming (CLR) produces syngas through the partial oxidation of methane. CLR takes place when oxygen is intentionally limited in order to force unreacted fuel or combustion products to react with water to form hydrogen. Reactions for CLR are of the form (Adanez et al., 2012):



with other side reactions possible. Reaction A.5 is strongly endothermic, requiring heat for the reaction to progress to be provided by alternate means if the heat produced by Reaction A.4 is

unable to be utilized for fully heating the reactor (Adanez et al., 2012). A possible method of providing this heat is by using CLC to heat the CLR reactor.

References

- Adanez, J; Abad, A; Garcia-Labiano, F; Gaya, P.; de Diego, L. F. Progress in Chemical-looping combustion and reforming technologies. *Prog. Energy Combust. Sci.* **2012**, *38*, 215-282.
- El-Bousiffi, M. A.; Gunn, D. J. A dynamic study of steam-methane reforming. *Int. J. Heat Mass Transfer* **2007**, *50*, 723-733.
- Molburg, J. C.; Doctor, R. D.; Hydrogen from steam-methane reforming with CO₂ capture. Proceedings of 20th Annual International Pittsburg Coal Conference, Pittsburg, PA; National Energy Technology Laboratory: 2003.
- Oliveira, E. L. G.; Grande, C. A.; Rodrigues, A. E. Methane reforming in large pore catalyst. *Chem. Eng. Sci.* **2010**, *65*, 1539-1550.

Appendix B: Heats of Reactions

As a preliminary step to the simulation determine an operating temperature that would lead to favorable reaction conditions. An overall chemical looping cycle, including a single reduction and then a single oxidation phase, was desired to be exothermic. This condition was chosen in order to allow the endothermic oxidation phase to be driven by the heat produced during the exothermic reduction phase.

Table B.1: Reaction Names (Iiuta et al., 2010; Dueso et al., 2012).

Name	Reaction
r_{s1}	$CH_4 + 2NiO \rightarrow 2Ni + 2H_2 + CO_2$
r_{s2}	$H_2 + NiO \rightarrow Ni + H_2O$
r_{s3}	$CO + NiO \rightarrow Ni + CO_2$
r_{s4}	$CH_4 + NiO \rightarrow Ni + 2H_2 + CO$
r_{o1}	$Ni + \frac{1}{2}O_2 \rightarrow NiO$

Table B.3: Reaction Stoichiometric Coefficients

Phase	Reaction	Coefficient CO ₂	Coefficient H ₂ O	Coefficient H ₂	Coefficient CO	Coefficient CH ₄	Coefficient O ₂	Coefficient NiO	Coefficient Ni
Reduction	r_{s1}	1	0	2	0	-1	0	-2	2
	r_{s2}	0	1	-1	0	0	0	-1	1
	r_{s3}	1	0	0	-1	0	0	-1	1
	r_{s4}	0	0	2	1	-1	0	-1	1
	overall	2	1	3	0	-2	0	-5	5
Oxidation	r_{o1}	0	0	0	0	0	-0.5	1	-1

Heat capacity of a substance at a certain temperature can be found from

$$\frac{C_p}{R} = A + BT + CT^2 + DT^{-2} \quad (B.1)$$

where T is in K and $R = 8.314 \frac{J}{mol \cdot K}$.

Table B.4: Heat Capacity Constants (Perry & Green, 2008; Smith et al., 2005).

Species	A	B	C	D
CO ₂	5.457	1.05E-03	0	-1.16E+05
H ₂ O	3.47	1.45E-03	0	1.21E+04
H ₂	3.249	4.22E-04	0	8.30E+03
CO	3.376	5.57E-04	0	3.10E+03
CH ₄	1.702	9.08E-03	-2.16E-06	0
O ₂	3.639	5.06E-04	0	-2.27E+04
NiO	11.3	2.15E-03	0	0
Ni	6.99	9.05E-04	0	0

Table B.5: Heat Capacities of Reaction Species at Various Temperatures.

Species	Heat Capacity at 298 K [J/mol K]	Heat Capacity at 873 K [J/mol K]	Heat Capacity at 1200 K [J/mol K]
CO ₂	3.71E+01	5.17E+01	5.51E+01
H ₂ O	3.36E+01	3.95E+01	4.34E+01
H ₂	2.88E+01	3.02E+01	3.13E+01
CO	2.97E+01	3.21E+01	3.36E+01
CH ₄	3.51E+01	6.63E+01	7.88E+01
O ₂	2.94E+01	3.37E+01	3.52E+01
NiO	9.93E+01	1.10E+02	1.15E+02
Ni	6.04E+01	6.47E+01	6.71E+01

The enthalpy change of a substance can be found from

$$\Delta H = C_p \Delta T \quad (B.2)$$

The enthalpy of CO₂ at 873 K is

$$\Delta H_{873K} = C_p^{873K} (873 K - 298 K) = 517 \frac{J}{mol \cdot K} (873 K - 298 K) = 29700 \frac{J}{mol}$$

with other species and temperatures following similarly.

Table B.6: Enthalpies of Reaction Species at Various Temperatures.

Species	Enthalpy at 873 K [J/mol]	Enthalpy at 1200 K [J/mol]
CO ₂	2.97E+04	4.97E+04
H ₂ O	2.27E+04	3.91E+04
H ₂	1.73E+04	2.82E+04
CO	1.85E+04	3.03E+04
CH ₄	3.82E+04	7.11E+04
O ₂	1.94E+04	3.17E+04
NiO	6.30E+04	1.04E+05
Ni	3.72E+04	6.06E+04

Table B.7: Standard Enthalpies of Formation of Reaction Species (Perry & Green, 2008; Smith et al., 2005).

Species	Standard Enthalpy of Formation [J/mol]
CO ₂	-393509
H ₂ O	-241818
H ₂	0
CO	-110525
CH ₄	-74520
O ₂	0
NiO	-244346
Ni	0

Enthalpy of formation for a temperature other than standard conditions can be found by

$$\Delta H_f = \Delta H^o + \Delta H \quad (B.3).$$

The enthalpy of formation of CO₂ at 873 K is

$$\Delta H_f^{873 K} = \Delta H_f^o + \Delta H^{873 K} = -393509 \frac{J}{mol} + 29700 \frac{J}{mol} = -364000 \frac{J}{mol}$$

with other species and temperatures following similarly.

Table B.8: Enthalpy of Formations of Reaction Species at Various Temperatures.

Species	Enthalpy of Formation at 873 K [J/mol]	Enthalpy of Formation at 1200 K [J/mol]
CO ₂	-3.64E+05	-3.44E+05
H ₂ O	-2.19E+05	-2.03E+05
H ₂	1.73E+04	2.82E+04
CO	-9.20E+04	-8.02E+04
CH ₄	-3.64E+04	-3.40E+03
O ₂	1.94E+04	3.17E+04
NiO	-1.81E+05	-1.40E+05
Ni	3.72E+04	6.06E+04

The overall enthalpy of reaction for a reaction is

$$\Delta H_{rxn i} = \sum_{j=1}^n \alpha_j \Delta H_{f,j} \quad (B.4).$$

The enthalpy of reaction r_{s1} at 873 K is

$$\begin{aligned}
\Delta H_{rxn,r_{s1}}^{873 K} &= \alpha_{CO_2} \Delta H_{f,CO_2}^{873 K} + \alpha_{H_2O} \Delta H_{f,H_2O}^{873 K} + \alpha_{H_2} \Delta H_{f,H_2}^{873 K} + \alpha_{CO} \Delta H_{f,CO}^{873 K} + \alpha_{CH_4} \Delta H_{f,CH_4}^{873 K} + \alpha_{NiO} \Delta H_{f,NiO}^{873 K} + \alpha_{Ni} \Delta H_{f,Ni}^{873 K} \\
&= 1 * -364000 + 0 * -219000 + 2 * 107300 + 0 * -90200 + -1 * -36400 + -2 * -181000 + 2 * 37200 \\
&= 144364 \frac{J}{mol} * \frac{kJ}{1000 J} = 144.364 \frac{kJ}{mol}
\end{aligned}$$

with other reactions and temperatures following similarly.

The enthalpy of the overall reduction phase is given as

$$\Delta H_{rxn,r_{overall}} = \sum_{i=1}^n \Delta H_{rxn,i} \quad (B.5).$$

The overall enthalpy of reaction of the complete chemical looping cycle is given as

$$\Delta H_{rxn,overall} = \Delta H_{rxn,r_{overall}} + \Delta H_{rxn,r_{o1}} \quad (B.6).$$

Table B.9: Enthalpies of Reactions for Various Temperatures

Reaction	Enthalpy Reaction at 298 K [kJ/mol]	Enthalpy of Reaction at 873 K [kJ/mol]	Enthalpy of Reaction at 1200 K [kJ/mol]
r _{s1}	169.7022	144.3644755	117.6721
r _{s2}	2.5276	-17.90186514	-30.0698
r _{s3}	-38.6384	-53.19871294	-62.7852
r _{s4}	208.3406	197.5631885	180.4573
Overall reduction	341.932	270.8270859	205.2745
r _{o1}	-244.346	-228.2284131	-216.683
Looping Overall	97.5864	42.59867279	-11.4081

References

- Dueso, C.; Ortiz, M.; Abad, A.; Garcia-Labiano, F.; de Diego, L. F.; Gayan, P.; Adanez, J. Reduction and oxidation kinetics of nickel-based oxygen carriers for chemical-looping combustion and chemical-looping reforming. *Chem. Eng. J.* **2012**, *188*, 142-154.
- Iliuta, I.; Tahoces, R.; Patience, G. S.; Rifflart, S.; Luck, F. Chemical-looping combustion process: Kinetics and mathematical modeling. *AIChE J.* **2010**, *56*, 1063-1079.
- Perry, R.; Green, D. Properties of formation and combustion reactions. *Perry's Chemical Engineers' Handbook*, Eighth edition; McGraw-Hill: 2008.
- Perry, R.; Green, D. Specific heats of pure compounds. *Perry's Chemical Engineers' Handbook*, Eighth edition; McGraw-Hill: 2008.
- Smith, J. M.; Van Ness, H. C.; Abbott, M. M. Appendix C. Heat capacities and property changes of formation. *Introduction to chemical engineering thermodynamics*, Seventh edition; McGraw-Hill: New York, 2005.